ΕΘΝΙΚΟ ΜΕΤΣΟΒΙΟ ΠΟΛΥΤΕΧΝΕΙΟ

ΣΧΟΛΗ ΕΦΑΡΜΟΣΜΕΝΩΝ ΜΑΘΗΜΑΤΙΚΩΝ ΚΑΙ ΦΥΣΙΚΩΝ ΕΠΙΣΤΗΜΩΝ

ΣΧΟΛΗ ΜΗΧΑΝΟΛΟΓΩΝ ΜΗΧΑΝΙΚΩΝ

ΕΚΕΦΕ «ΔΗΜΟΚΡΙΤΟΣ»

ΙΝΣΤΙΤΟΥΤΟ ΝΑΝΟΕΠΙΣΤΗΜΗΣ ΚΑΙ ΝΑΝΟΤΕΧΝΟΛΟΓΙΑΣ

ΙΝΣΤΙΤΟΥΤΟ ΠΥΡΗΝΙΚΗΣ ΚΑΙ ΣΩΜΑΤΙΔΙΑΚΗΣ ΦΥΣΙΚΗΣ

Διατμηματικό Πρόγραμμα Μεταπτυχιακών Σπουδών

«Φυσική και Τεχνολογικές Εφαρμογές»

SEARCH FOR SINGLY PRODUCED b* DECAYING TO tW IN THE LEPTON+JETS (LEPTONIC W + HADRONIC TOP) CHANNEL WITH CMS DETECTOR AT sqrt{s} = 13 TeV

Αναζήτηση μεμονωμένων σωματιδίων b* στο κανάλι διάσπασης tW, με υπογραφή λεπτονίου και αδρονικών πιδάκων, με τον ανιχνευτή CMS σε συγκρούσεις πρωτονίων ενέργειας κέντρου μάζας 13 TeV

ΜΕΤΑΠΤΥΧΙΑΚΗ ΔΙΠΛΩΜΑΤΙΚΗ ΕΡΓΑΣΙΑ

της Ναυσικάς Καλογεροπούλου

Επιβλέπων:
Κώστας Κουσουρής

Αθήνα, Ιούλιος, 2023

Abstract

A search for a heavy resonance decaying into a top quark and a W boson in proton-proton collisions at $\sqrt{s} = 13$ TeV is presented. The data analyzed were recorded with the CMS detector at the LHC and correspond to an integrated luminosity of 36.3 fb^{-1}. The analysis is focused on the semileptonic final state, where the W boson decays leptonically and reconstructed as a lepton (μ) and a missing transverse momentum, while the top quark decays hadronically and reconstructed as a jet identified as originating from a bottom quark and as two jets with invariant mass equal to the W boson mass. An excited bottom quark b^* model is used as a benchmark during the search. The hypotheses of b^* quarks with left-handed chirality are excluded at 90% confidence level for masses below 2.2 TeV.

Εκτεταμένη περίληψη

Αναζήτηση για μεμονωμένο βαρύ συντονισμό b^* στο κανάλι διάσπασης tW σε συγρούσεις πρωτονίων ενέργειας κέντρου μάζας 13 TeV παρουσιάζεται. Τα δεδομένα συλλέχθηκαν με τον ανιχνευτή CMS με συνολική φωτηνότητα 36.3 fb^{-1}. Η ανάλυση εστιάζει στην ημιλεπτονική τελική κατάσταση, όπου το W μποζόνιο διασπάται λεπτονικά και ανακατασκευάζεται ως λεπτόνιο (μ) και ως ελλείπουσα εγκάρσια ορμή, ενώ το top κουαρκ διασπάται αδρονικά και ανακατασκευάζεται ως 3 αδρονικοί πίδακες εκ των οποίων ο ένας προέρχεται από αδρονοποίηση b κουαρκ.

Τα δεδομένα περιγράφονται καλύτερα με το υπάρχον φυσικό μοντέλο (Καθιερωμένο Πρότυπο), δηλαδή δεν δίνουν ένδειξη για την ύπαρξη του βαρύ συντονισμού b^*. Αφού το πείραμα έχει δώσει αρνητικό αποτέλεσμα για την ύπαρξη του b^*, αυτό που προσπαθήσαμε να κάνουμε στην παρούσα πτυχιακή εργασία ήταν να θέσουμε ένα άνω όριο στην ενεργό διατομή παραγωγής του b^* για διάφορες υποτιθέμενες μάζες. Άνω όριο σημαίνει ότι αν το b^* σωμάτιο υπήρχε, τότε θα παραγόταν με ενεργό διατομή μικρότερη από άνω όριο που θέσαμε.

Για να θέσουμε το άνω όριο χρησιμοποιήσαμε την μέθοδο CLs, που είναι η πλέον διαδεδομένη μέθοδος για την περίπτωση που το σήμα είναι πολύ μικρό σε σχέση με το υπόβαθρο. Για μια συγκεκριμένη υποτιθέμενη μάζα του b^* θεωρήσαμε μοντέλα σήματος+υποβάθρου που διαφέρουν στην ενεργό διατομή παραγωγής του βαρύ συντιονισμού και τα συγκρίναμε με το μοντέλο του υποβάθρου. Τα μοντέλα σήματος+υποβάθρου, και συνεπώς οι αντίστοιχες ενεργός διατομές, που δεν ικανοποίησαν τα κριτήρια του στατιστικού τεστ τα αποκλείσαμε, και έτσι κατασκευάσαμε από την μεγαλύτερη μη αποκλισμένη τιμή της ενεργού διατομής άνω όριο. Την ίδια διαδικασία επαναλάβαμε για διαφορετικές υποτιθέμενες μάζες του b^*.

Ευχαριστίες

Θα ήθελα να ευχαριστήσω τον επιβλέποντα καθηγητή μου, κ. Κωνσταντίνο Κουσουρή, για όλη τη βοήθεια, την στήριξη και τις γνώσεις που μου προσέφερε καθόλη τη διάρκεια της ενασχόλησης μου με την διπλωματική εργασία. Επίσης, ευχαριστώ και όλα τα μέλη της ομάδας του CMS στο Εθνικό Μετσόβιο Πολυτεχνείο για την βοήθεια και τις συμβουλές που μου παρείχαν.

Contents

Introduction

1.1 Standard Model overview

The Standard Model of particle physics is the theory describing three of the four known fundamental forces (electromagnetic, weak and strong interactions - excluding gravity) in the universe and classifying all known elementary particles.

It includes 12 elementary particles of spin 1/2, known as fermions. According to the spin-statistics theorem, fermions respect the Pauli exclusion principle. Each fermion has a corresponding antiparticle.

Fermions are classified according to how they interact. There are 6 quarks (up, down, charm, strange, top, bottom) and 6 leptons (electron, electron neutrino, muon, muon neutrino, tau, tau neutrino). Each class is divided into pairs of particles that exhibit a similar physical behavior called a generation; up and down quarks - electron and electron neutrino made up the first generation; charm and strange quarks - muon and muon neutrino made up the second generation; top and bottom quarks - tau and tau neutrino made up the third generation.

The defining property of quarks is that they carry color charge, and hence interact via the strong interaction. The phenomenon of color confinement results in quarks being very strongly bound to one another, forming color-neutral composite particles called hadrons that contain either a quark and an antiquark (mesons) or three quarks (baryons). Quarks also carry electric charge and weak isospin. Hence they interact with other fermions via electromagnetism and the weak interaction. The leptons do not carry color charge, and the three neutrinos do not carry electric charge either so their motion is directly influenced by the weak force; while the other leptons by virtue of carrying an electric charge interact electromagnetically.

Each member of a generation has a greater mass than the corresponding

particle of any generation before it. The first generation charged particles do not decay, hence all ordinary (baryonic) matter is made of such particles. Neutrinos of all generations also do not decay, and pervade the universe, but rarely interact with baryonic matter.

Gauge bosons are defined as force carriers that mediate the strong, weak and electromagnetic interactions. Within the Standard Model the forces are explained as resulting from matter particles exchanging other particles, referred to as force mediating particles. Their spin value is 1 which is making them bosons. As a result they do not follow the Pauli exclusion principle that constrains fermions; bosons do not have a theoritical limit on their spatial density.

Photons mediate the electromagnetic force between charged particles. The W^+, W^- and Z gauge bosons mediate the weak interactions between particles of different flavor. The eight gluons mediate the strong interaction between the quarks. The eightfold multiplicity of gluons is labeled by a combination of color and anticolor charge. Because gluons have an effective color charge, they can also interact among themselves. Finally, the Higgs particle is a massive scalar elementary particle. It plays a unique role in the Standard Model by explaining why the other elementary particles, except the photon and gluon, are massive, and why the above two are massless.

A figure illustrating the classification of the elementary particles within the Standard Model is shown below. To each a value of its mass and its electric charge in units of the electron charge has been attached.

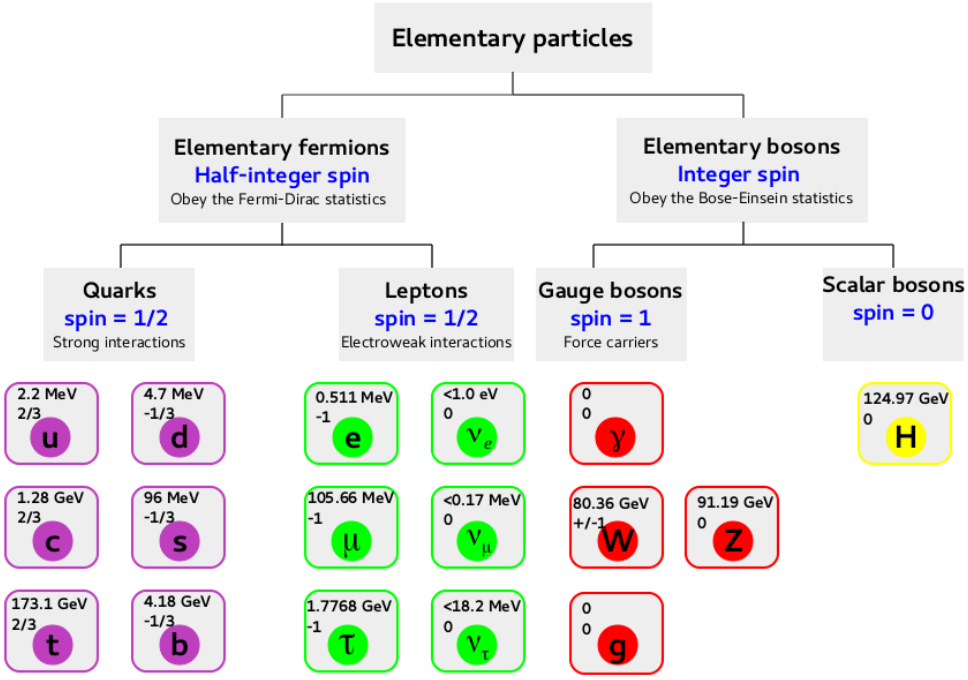

Figure 1.1: Classification of the elementary particles within the Standard Model

Let's start with quarks, and in particular with the two types of quarks up and down. Up and down quark can be either "left-handed" or "right-handed" depending on whether they are spinning clockwise or counterclockwise with respect to their direction of motion.

Left-handed up and down quarks can transform into each other, via the weak force – the quarks exchange a W boson. This weak interactions are represented by orange lines, as shown in the figure below. Strangely, there are no right-handed W bosons in nature. This means right-handed up and down quarks cannot emit or absorb W bosons, so they don't transform into each other.

Figure 1.2: Weak force

Quarks also possess a kind of charge called color. A quark can have either red, green or blue color charge. A quark's color makes it sensitive to the strong force. The strong force binds quarks of different colors together into composite particles such as protons and neutrons, which are "colorless", with no net color charge. Quarks transform from one color to another by absorbing or emitting particles called gluons, the carriers of the strong force. These interactions form the sides of a triangle, as shown below. Because gluons possess color charge themselves, they constantly interact with one another as well as with quarks. The interaction between gluons fill the triangle in.

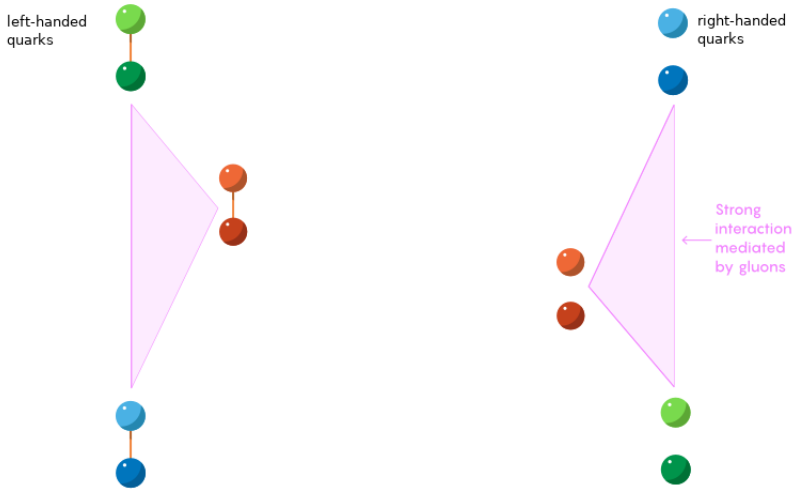

Figure 1.3: Strong force

Leptons come in two types: electrons which have an electric charge of -1 and neutrinos which are electrically neutral. As with left-handed up and down quarks, left-handed electrons and neutrinos can transform into each

other via the weak interaction. However, right-handed neutrinos have not been seen in nature. The main feature that distinguishes leptons from quarks is that they do not interact via the strong force.

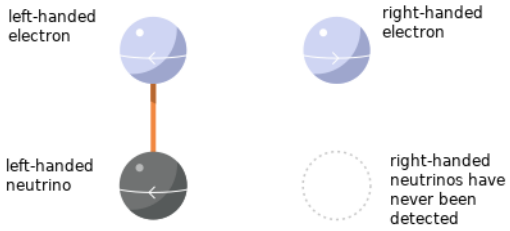

Figure 1.4: Leptons – right-handed components of neutrinos have not been observed

For unknown reasons, three progressively heavier but otherwise identical versions of each type of matter particle exist. Along with the up and down quark, there is the charm and strange quark and, heavier still, the top and the bottom quark. The same is true for leptons: along with the electron and the electron neutrino, there are the muon and muon neutrino and the tau and tau neutrino.

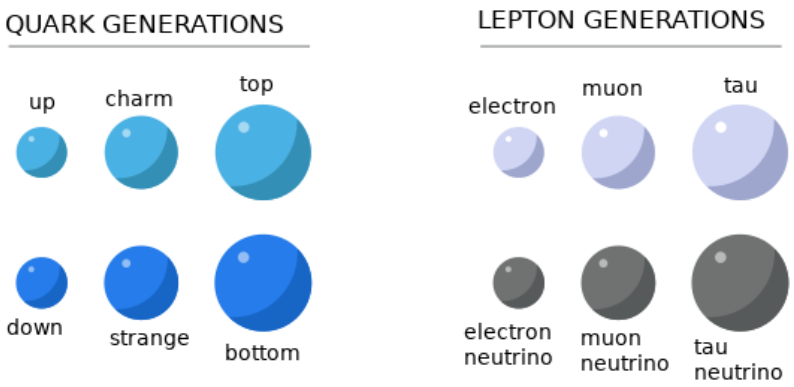

Figure 1.5: Quark generations (left) and lepton generations (right)

A small amount of weak interaction happens between left-handed quarks in different generations, so that an up quark could occasionally spit out a

W^+ boson and become a strange quark, for example. Leptons in different generations have not been seen interacting in this manner.

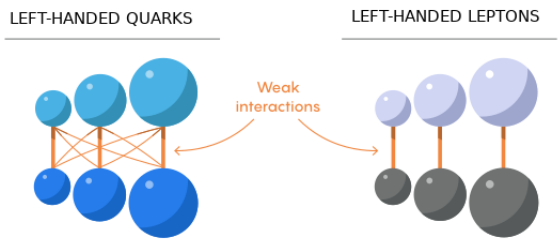

Figure 1.6: Weak interaction between left-handed quarks in different generations. Weak interaction between left-handed leptons in different generations have not been observed.

All matter particles except for neutrinos have electric charge, therefore they are sensitive to the electromagnetic force. They interact with one another by exchanging photons, the carriers of the electromagnetic force. We represent electromagnetic interactions as wavy lines. These interactions do not transform particles into one another; in this case, particles just feel a push or pull.

Aside from the W^+ and W^- bosons, there is also a neutral carrier of the weak force, called the Z^0 boson. Particles can absorb or emit Z^0 bosons without changing identities, merely losing or gaining energy and momentum. Weak neutral interactions are represented by orange wavy lines.

Finally, the Higgs boson is the linchpin of the Standard Model. In general, the more a particle interacts with the Higgs boson, the more mass it has.

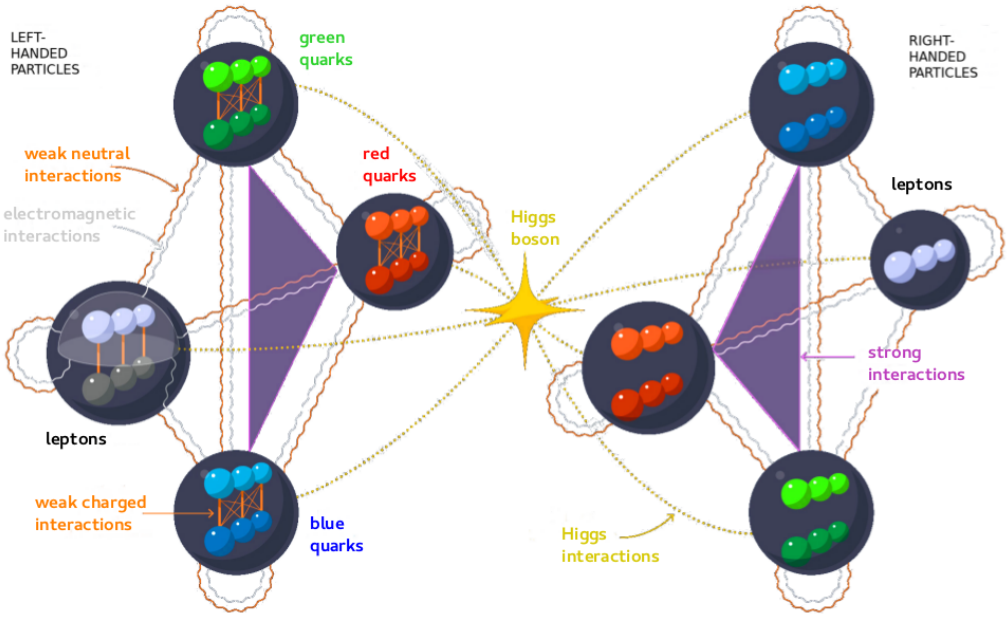

Figure 1.7: An illustrative picture of the Standard Model particles and interactions

1.2 A more detailed description of the SM

The Standard Model is a mathematical model for describing the behavior of the elementary particles and their strong, weak and electromagnetic interactions in terms of "gauge theories". A gauge theory is one that possesses invariance under a set of "local transformations" i.e. transformations whose

parameters are space-time dependent. Electromagnetism is a gauge theory associated with the the group $U(1)_{em}$. In this case the gauge transformations are local complex phase transformations of the fields of charged particles. Gauge invariance necessitates the introduction of a massless vector (spin-1) particle, the photon. Yang and Mills considered extending gauge invariance to include local non-Abelian transformations such as $SU(2)$. In $SU(2)$ one needs 3 massless vector fields to preserve gauge invariance. However, weak interactions are known to be mediated by 3 massive vector bosons. This is solved by the "Higgs mechanism", a scalar potential that is added to the Lagrangian to generate the vector-boson (and fermion) masses in a gauge invariant way. A remnant scalar field, the Higgs boson is part of the physical spectrum. The gauge theory of strong interactions is called Quantum ChromoDynamics associated with the group $SU(3)_C$. Quarks possess an internal property called "color" and the gauge transformations are local transformations between quarks of different colors.

1.2.1 QED

Lets start from the Dirac free Lagrangian describing a fermion

$$\mathcal{L}_\psi = \bar{\psi}(i\gamma^\mu \partial_\mu - m)\psi$$

and the local gauge transformation

$$\psi \to e^{-i\alpha(x)}\psi$$

If we introduce the gauge field A_μ through the minimal coupling

$$D_\mu = \partial_\mu + ieA_\mu$$

and at the same time, require that A_μ transforms like

$$A_\mu \to A_\mu + \frac{1}{e}\partial_\mu \alpha$$

then we have the local $U(1)$ gauge invariant Lagrangian that describes Quantum Electrodynamics:

$$\mathcal{L}_{QED} = \bar{\psi}(i\gamma^\mu \partial_\mu - m)\psi - e\bar{\psi}\gamma^\mu A_\mu \psi - \frac{1}{4}F_{\mu\nu}F^{\mu\nu}$$

The electromagnetic strength tensor, $F_{\mu\nu} = \partial_\mu A_\nu - \partial_\nu A_\mu$, accounts for the kinetic energy of the photon and is invariant under the gauge transformation.

1.2.2 Electroweak interactions

The gauge group which unifies and describes the electromagnetic and weak interactions is $SU(2)_L \otimes U(1)_Y$, where the subscript Y denotes hypercharge, which is related to the electric charge Q and the the weak isospin T_3 via the relation

$$Q = T_3 + \frac{1}{2}Y$$

Left-handed leptons are placed in weak isospin doublets $L = \begin{pmatrix} \nu \\ l \end{pmatrix}_L$, while right-handed leptons in weak isospin singlets $R = l_R$, since there is no right-handed component for the neutrino. Next step is to introduce gauge fields corresponding to each generator:

$$SU(2)_L \rightarrow W^1_\mu, W^2_\mu, W^3_\mu$$
$$U(1)_Y \rightarrow B_\mu$$

and the fermion-gauge boson coupling via the covariant derivative:

$$L : \partial_\mu + i\frac{g}{2}\tau^i W^i_\mu + i\frac{g'}{2}Y B_\mu$$
$$R : \partial_\mu + i\frac{g'}{2}Y B_\mu$$

where g and g' are the coupling constants associated to the groups $SU(2)_L$ and $U(1)_Y$ respectively, and $Y_{L_l} = -1, Y_{R_l} = -2$. Therefore the Lagrangian becomes:

$$\mathcal{L} = \bar{R}i\gamma^\mu\partial_\mu R + \bar{L}i\gamma^\mu\partial_\mu L + \bar{L}i\gamma^\mu(i\frac{g}{2}\tau^i W^i_\mu + i\frac{g'}{2}YB_\mu)L$$
$$+ \bar{R}i\gamma^\mu(i\frac{g'}{2}YB_\mu)R - \frac{1}{4}W^i_{\mu\nu}W^{i\mu\nu} - \frac{1}{4}B_{\mu\nu}B^{\mu\nu}$$

where the first two and last two terms are the free Lagrangian of leptons and gauge fields respectively and the middle terms are the fermion-gauge boson interactions. The charged weak bosons appear as a linear combination of W^1 and W^2, while the photon and the neutral Z are both given by a mixture of W^3 and B.

Up to now we have in the theory 4 massless gauge fields and 2 massless fermions. The next step will be to add scalar fields in order to break spontaneously the symmetry and use the Higgs mechanism to give mass to the three weak intermediate vector bosons and to the leptons.
So we introduce the scalar Higgs doublet $\Phi = \begin{pmatrix}\phi^+\\ \phi^0\end{pmatrix}$ and the Lagrangian

$$\mathcal{L}_{scalar} = \partial_\mu\Phi^\dagger\partial^\mu\Phi - V(\Phi^\dagger\Phi)$$

where the potential is given by

$$V(\Phi^\dagger\Phi) = \mu^2\Phi^\dagger\Phi + \lambda(\Phi^\dagger\Phi)^2$$

In order to maintain the gauge invariance under the $SU(2)_L \otimes U(1)_Y$ we have to replace the normal with the covariant derivative. We can choose the vacuum expectation value of the Higgs field as (i.e. spontaneously break the symmetry of the Lagrangian)

$$< \Phi >_0 = \begin{pmatrix}0\\ \upsilon/\sqrt{2}\end{pmatrix}, \upsilon = \sqrt{-\frac{\mu^2}{\lambda}}$$

Let us parametrize the Higgs doublet

$$\Phi = e^{i\frac{\tau^i}{2}\frac{\chi_i}{v}} \begin{pmatrix} 0 \\ (v+H)/\sqrt{2} \end{pmatrix}$$

If we make a $SU(2)_L$ gauge transformation with $\alpha_i = \frac{\chi_i}{v}$, the fields and the Lagrangian become

$$\Phi \to \Phi' = \frac{(v+H)}{\sqrt{2}} \begin{pmatrix} 0 \\ 1 \end{pmatrix}$$

$$\mathcal{L}'_{scalar} = |(\partial_\mu + ig\frac{\tau^i}{2}W^i_\mu + i\frac{g'}{2}YB_\mu)\frac{(v+H)}{\sqrt{2}}\begin{pmatrix} 0 \\ 1 \end{pmatrix}|^2 - \mu^2\frac{(v+H)^2}{2} - \lambda\frac{(v+H)^4}{4}$$

from which after some algebra we can identify the masses of the 3 vector bosons and the mass of the Higgs boson (H).
The next step is to give mass to the charged leptons in a gauge invariant way via the Yukawa coupling of the leptons with the Higgs field

$$\mathcal{L}_{Yuk} = -G_l[\bar{R}(\Phi^\dagger L) + (\bar{L}\Phi)R]$$

Thus

$$M_l = \frac{G_l v}{\sqrt{2}}$$

This procedure though does not specify the value of the mass since the Yukawa constant G_l introduced is arbitrary.

Electroweak interactions of quarks and their masses can be introduced in a similar way as for leptons. The weak isospin doublets of quarks are

$$\begin{pmatrix} u \\ d' \end{pmatrix}, \begin{pmatrix} c \\ s' \end{pmatrix}, \begin{pmatrix} t \\ b' \end{pmatrix}$$

where the quark mixing, by convention is restricted to the down quarks:

$$\begin{pmatrix} d' \\ s' \\ b' \end{pmatrix} = (CKM matrix) \begin{pmatrix} d \\ s \\ b \end{pmatrix}$$

1.2.3 QCD

Starting from the Dirac free Lagrangian describing the quark color fields

$$\mathcal{L}_q = \bar{q}(i\gamma^\mu \partial_\mu - m)q$$

and the local $SU(3)$ gauge transformation

$$q \to e^{-i\alpha_\alpha(x)T_\alpha} q$$

If we introduce eight gauge fields G^α_μ, which are the so called gluons, through the covariant derivative

$$D_\mu = \partial_\mu + igT_\alpha G^\alpha_\mu$$

each transforming as

$$G^\alpha_\mu \to G^\alpha_\mu - \frac{1}{g}\partial_\mu \alpha^\alpha - f_{\alpha bc}\alpha_b G^c_\mu$$

where $f_{\alpha bc}$ are real constants, called the structure constant of the group,and we add a gauge invariant kinetic energy term for each of the G^α_μ field, then we have a local $SU(3)$ gauge invariant Lagrangian that describes strong interactions

$$\mathcal{L}_{QCD} = \bar{q}(i\gamma^\mu \partial_\mu - m)q - g(\bar{q}\gamma^\mu T_\alpha q)G^\alpha_\mu - \frac{1}{4}G^\alpha_{\mu\nu}G^{\mu\nu}_\alpha$$

The most important phenomena in QCD are asymptotic freedom and confinement – the quarks and gluons appear as free particles only at very short distances, probed in deep-inelastic scattering, but are confined into mesons and baryons at large distances.

1.3 Beyond the SM

Despite being the most successful theory of particle physics to date, the Standard Model is not perfect. There are fundamental physical phenomena in nature that the Standard Model does not adequately explain: **Gravity is not included**. Moreover, the SM is widely considered to be incompatible with the theory of gravity, general relativity. **Dark matter and dark energy**. Cosmological observations tell us the SM explains about 5% of the mass-energy present in the universe. About 26% should be dark matter and the remaining 69% dark energy. **Neutrino masses**. According to the SM, neutrinos are massless particles, however, neutrino oscillation experiments have shown that neutrinos do have mass. **Matter-antimatter asymmetry**. The universe is made out of mostly matter. However, the SM predicts that matter and antimatter should have been created in equal amounts.

Supersymmetry is an extension of the SM that aims to fill some of the gaps. Supersymmetry is a spacetime symmetry between two basic classes of particles: bosons, which have an integer-valued spin, and fermions, which have a half-integer-valued spin. In supersymmetry, each particle from one class would have an associated particle in the other, known as its superpartner, the spin of which differs by a half-integer. In the simplest supersymmetry theories, with perfectly "unbroken" supersymmetry, each pair of superpartners would share the same mass and internal quantum numbers besides spin. More complex supersymmetry theories have a spontaneously broken symmetry, allowing superpartners to differ in mass. In the SM the strengths of the three forces change as a function of energy, and become closer to each other at very high energies. In SM together with supersymmetry (Minimal Supersymmetric Standard Model), however, they become equal within a percent-level accuracy.

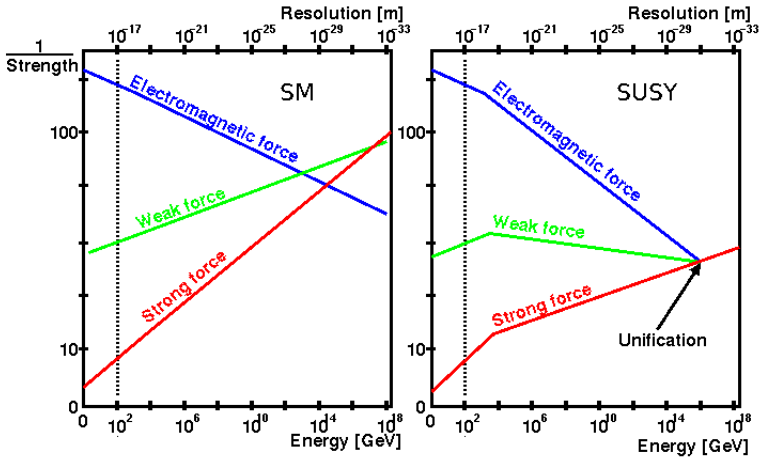

Figure 1.8: Running of the three coupling constants in the SM (left) and in SUSY (right)

Many possibilities for physics beyond the SM have been proposed, including the possibility that quarks are composite. Such quarks would have an intern structure that, excited, could produce a state with higher mass. CMS continues to probe the existence of a substructure to the so-called "fundamental particles". One such search performed by the CMS looks for an excited bottom quark. If a quark is made up of other constituent particles, the energy required to split them would be higher than the energies provided by the LHC. However, it may be possible to "excite" the bottom quark in a way similar to an electron being excited to a higher orbit in an atom by the absorption of a photon. A quark could instead be excited by the absorption of a gluon, as these are abundant in the proton collisions made by the LHC. In such an interaction, the energy of a gluon would be converted into internal energy of a bottom quark which would then appear as a very heavy particle, called an excited bottom quark. The new particle would be so massive that any decay to two standard model particles will result in vast amounts of binding energy being transferred to the lighter decay products as kinetic energy. In that case, such a new particle would create a back-to-back signature with the decay particles in opposite hemispheres of the detector.

Because we do not know the mass of the excited bottom quark, scenarios with excited bottom quarks of different masses and predictive models are compared against the background-only model. The statistical analysis of

the data checks if one of these models describes the data better than the background-only model. If the model with a signal does not reproduce the data significantly better than the background alone, we instead set a limit on our sensitivity to detect excited bottom quarks below a certain mass.

Collider Physics

2.1 LHC

The LHC is the world's largest and highest-energy particle accelerator. It is installed in an underground tunnel of 27 km circumference. The accelerator is a succession of machines with increasingly higher energies. Each machine accelerates a beam of particles to a given energy before injecting the beam into the next machine in the chain. This next machine brings the beam to an even higher energy and so on. The LHC is the last element of this chain, in which the beams reach their highest energies. Inside the LHC, two high-energy particle beams travel at close to the speed of light before they are made to collide at four locations, corresponding to the positions of four particle detectors – ATLAS, CMS, ALICE and LHCb.

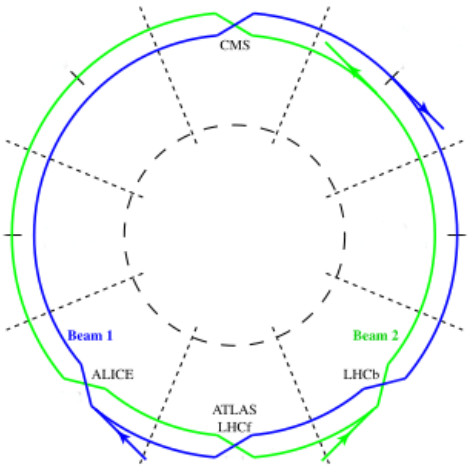

Figure 2.1: Schematic layout of the LHC with its two-beam design and its four experimental insertions

The beams travel in opposite directions in separate beam pipes - two tubes are kept at ultrahigh vacuum so that the beam does not crash into molecules in its path. They are guided around the accelerator ring by a strong magnetic field maintained by superconducting electromagnets. The beam consist of bunches of 10^{11} protons which are made to collide every 25 ns, corresponding to 1 billion collisions every second. Two beams of protons will each travel at a maximum energy of 7 TeV, corresponding to head-to-head collisions of 14 TeV. The key objective of the LHC is the exploration of the Standard Model in the TeV energy range and search for potential new physics signatures.

2.2 CMS

The Compact Muon Solenoid detector is shaped like an onion with several concentric layers of components. The innermost layer is a silicon-based tracker. Surrounding it is a scintillating crystal electromagnetic calorimeter, which is itself surrounded with a sampling calorimeter for hadrons. The tracker and the calorimetry are compact enough to fit inside the CMS solenoid. Outside the magnet are the large muon detectors, which are inside the return yoke of the magnet.

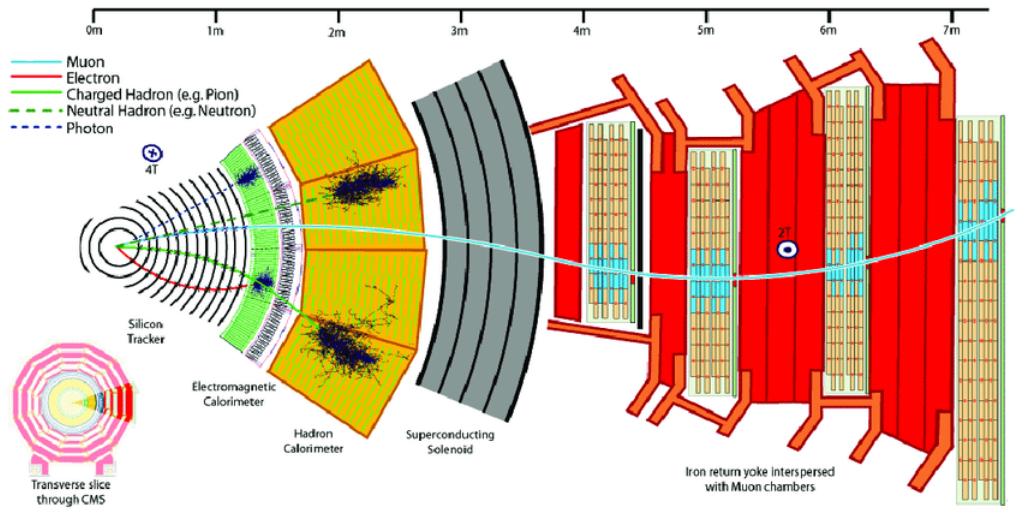

Figure 2.2: The Compact Muon Solenoid complex

CMS acts as a giant, high-speed camera, taking 3D "photographs" of particle collisions from all directions up to 40 million times each second. Although most of the particles produced in the collisions are unstable, they transform rapidly into stable particles that can be detected by the CMS. By identifying nearly all the stable particles produced in each collision, measuring their momenta and energies, and then piecing together the information of all these particles, the detector can recreate an "image" of the collision for further analysis. The components of the CMS help prepare "photographs" of each collision event by determining the properties of the particles produced. This is done by:

- Bending particles
  A powerful magnet is needed to bend charged particles as they fly outwards from the collision point. Bending the trajectories of the particles serves two purposes: helps to identify the charge of the particle - positively and negatively charged particles bend in opposite directions in the same magnetic field, and allows us to measure the momentum of the particle.
  The solenoid magnet is formed by a cylindrical coil of superconducting fibres. When electricity is circulating within these coils, they encounter no resistance (superconductivity) and can generate a magnetic field of

around 4 T. This high magnetic field must be confined to the volume of the detector and is done by the steel "yoke" that forms the bulk of the detector's mass. This solenoid is the largest magnet of its type ever constructed and allows the tracker and calorimeters to be placed inside the coil, resulting in a compact detector.

- Identifying tracks
  CMS must identify the paths taken by these bent charged particles with a very high precision. This is done by a silicon tracker made of around 75 million individual electronic sensors arranged in concentric layers. When a charged particle flies through the tracker layer, it interacts electromagnetically with the silicon and produces a hit – these individual hits can then be joined together to identify the track of the traversing particle.

- Measuring energy
  Information about the energies of the various particles produced in each collision is crucial to understanding what occurred at the collision point. This information is collected from two kinds of calorimeters. The electromagnetic calorimeter (ECAL) is the inner layer of the two and measures the energy of electrons and photons by stopping them completely. Hadrons, which are composite particles made up of quarks and gluons, fly though the ECAL and are stopped by the outer layer called the hadron calorimeter (HCAL).

- Detecting muons
  The final particle that the CMS observe directly is the muon. Muons are not stopped by the calorimeters, so special sub-detectors have to be built to detect them. These sub-detectors are interleaved with the return yoke of the solenoid. CMS is designed to detect muons very accurately and the large magnet also allows us to measure each muon's momentum both inside the superconducting coil (by the tracking devices) and outside of it (by the muon chambers).

2.3 Collider parameters and kinematic variables

The important parameters for designing a collider are the center-of-momentum energy of the beam, the instantaneous peak luminosity, the relative beam energy spread, the bunch crossing frequency, the number of particles per bunch and the total length of the collider. The instantaneous peak luminosity is the number of particles passing each other per unit time through unit transverse area at the interaction point. The particle beams usually come in bunches. If there are n_1 particles in each bunch in beam 1 and n_2 in each bunch in beam 2, then the collider luminosity scales as

$$\mathcal{L} \propto f n_1 n_2 / \alpha$$

where f is beam crossing frequency and α the transverse profile of the beams. The instantaneous luminosity is usually given in units of $\mathrm{cm}^{-2}\mathrm{s}^{-1}$.

Figure 2.3: Bunches of protons are made to collide with a time interval $t = 1/f$

The reaction rate, that is the number of scattering events per unit time, is given by

$$R(s) = \sigma(s)\mathcal{L}$$

where $\sigma(s)$ is defined to be the total scattering cross section. The total cross section for a pp scattering can be estimated by dimensional analysis to be about 100 mb, with weak energy dependence.

The limiting factor to the collider energy is the energy loss during the acceleration, known as the synchrotron radiation. For a circular machine of

radius R, the energy loss per revolution is $\Delta E \propto \frac{1}{R}(\frac{E}{m})^4$, where E is beam energy and m the particle mass. It becomes clear that an accelerator is more efficient for a larger radius or a more massive particle.

The CMS coordinate system is oriented such that the x axis points to the centre of the LHC ring, the y axis points vertically upward, and the z axis is the direction of the beam. The azimuthal angle ϕ is measured from the x axis in the (x,y) plane, and the radial coordinate in this place is denoted r. The polar angle θ is defined in the (r,z) plane with respect to the z axis.

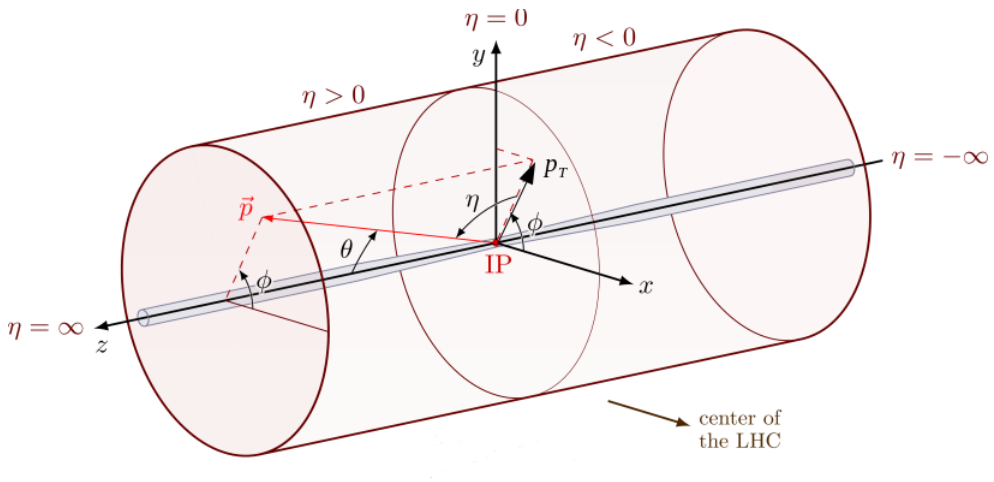

Figure 2.4: CMS coordinate system

The kinematic variables used are the component of the momentum transverse to the z axis, $p_T = \sqrt{p_x^2 + p_y^2}$, the pseudorapidity ($\eta$), which has one-to-one correspondence with the scattering polar angle $\pi \geq \theta \geq 0$ for $-\infty < \eta < \infty$, (rapidity defined as $y = \frac{1}{2} ln \frac{E+p_z}{E-p_z}$. In the massless limit, $E \approx |\vec{p}|$, so that $y \to \frac{1}{2} ln \frac{1+cos\theta}{1-cos\theta} = lncot\frac{\theta}{2} = \eta$), the angular distance between two object defined as $\Delta R = \sqrt{(\Delta\eta)^2 + (\Delta\phi)^2} = \sqrt{(\eta_1 - \eta_2)^2 + (\phi_1 - \phi_2)^2}$, the missing transverse momentum and the invariant mass. The neutrino cannot be directly observed by the detector and only its transverse momentum can be inferred by the imbalancing of the observed momenta, $\vec{\not{p}}_T = -\sum \vec{p_T}(observed)$ called missing transverse momentum, identified as $\not{p}_T = p_{\nu T}$. For the invariant mass, suppose a particle A decaying to particles B and C; then the

invariant mass of the decaying particle is defined as $m_A = \sqrt{(p_B + p_C)^2}$, where p_B and p_C are the four-momenta of the daughter particles.

2.4 Triggering

When CMS is performing at its peak, about one billion pp interactions will take place every second inside the detector. There is no way that data from all these events could be read out, and even if they could, most would be less likely to reveal new phenomena; they might be low-energy glancing collisions for instance, rather than energetic, head-on interactions. Therefore we need a trigger that can select the potentially interesting events and reduce the rate to just a few hundred events per second, which can be read out and stored on computer disk for subsequent analysis.

However, with groups of protons colliding 40 million times per second there are only ever 25 ns before the next lot arrive. The solution is to store the data in pipelines that can retain and process information from many interactions at the same time. To not confuse particles from two different events, the detectors must have very good time resolution and the signals from the millions of electronic channels must be synchronized so that they can all be identified as being from the same event.

The event rate is reduced in two steps called Level-1 (L1) Trigger and High-Level Trigger (HLT). L1 trigger is an extremely fast and wholly automatic process that looks for simple signs of interesting physics, e.g. particles with a large amount of energy or in unusual combinations. It uses coarsely segmented data from the calorimeters and the muon systems, while holding the high resolution data in pipelined memories. This way we select the best 100000 events each second from the billion available. In the HLT trigger, we assimilate and synchronize information from different parts of the detector to recreate the entire event and send it to a farm of more than 1000 standard computers. Here the PCs are like speed readers, who with more detailed information review the information for longer, less than a tenth of a second. They run complex physics tests to look for specific signatures, for instance matching tracks to hits in the muon chambers, or spotting photons through their high energy but lack of charge. Overall they select 100 events per second and the remaining 99900 are thrown out.

There are many means to design a trigger, such as particle identification, multiplicity, kinematics, event topology etc. Modern detectors usually

can trigger on muons by muon chambers, electrons/photons as electromagnetic objects, τ/hadrons and jets as hadronic objects, global energy sum and missing transverse energy, and some combinations of the above.

2.5 Muon reconstruction

Three types of gas ionization chambers were chosen to make up the CMS muon system: drift chambers (DTs), cathode strip chambers (CSCs) and resistive plate chambers (RPCs). The DTs are segmented into drift cells; the position of the muon is determined by measuring the drift time to an anode wire of a cell with a shaped electric field. The CSCs operate as standard multi-wire proportional counter but add a finely segmented cathode strip readout, which yields an accurate measurement of the position of the bending plane ($R - \phi$) coordinate at which the muon crosses the gas volume. The RPCs are double-gap chambers operated in avalanche mode and are primarily designed to provide timing information for the muon trigger.

The various muon stations within the CMS are shown below. We distinguish three regions, naturally defined by the cylindrical geometry of CMS, referred to as barrel ($|\eta| < 0.9$), overlap ($0.9 < |\eta| < 1.2$) and endcap ($1.2 < |\eta| < 2.4$) regions.

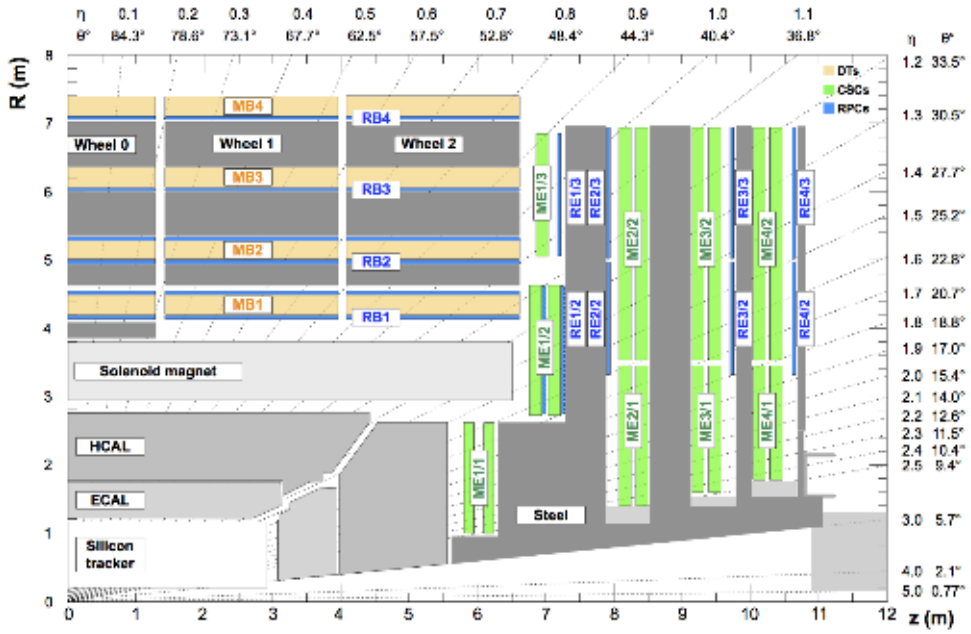

Figure 2.5: An R-z cross section of a quadrant of the CMS detector with the axis parallel to the beam (z) running horizontally and the radius (R) increasing upward. The interaction point is the lower left corner. The locations of the various muon stations and the steel flux-return disks (dark areas) are shown. The drift tubes stations are labeled MB ("Muon Barrel") and the cathode strip chambers are labeled ME ("Muon Endcap"). Resistive plate chambers are mounted in both the barrel and endcaps of CMS, where they are labeled RB and RE respectively.

Muons and other charged particles that traverse a muon subdetector ionize the gas in the chambers, which eventually causes electric signals to be produced on the wires and strips. These signals are read out by electronics and are associated with well-defined locations, generically called "hits", in the detector. The precise location of each hit is reconstructed using different algorithms.

Hit reconstruction in a DT drift cell specifies the transverse distance between the wire and the intersection of the muon trajectory with the plane containing the wires in the layer. The electrons produced through gas ionization by a muon crossing the cell are collected at the anode wire. A time-to-digital converter (TDC) registers their arrival time, T_{TDC}. This time is

then corrected by a time pedestal, T_{ped}, and multiplied by the electron drift velocity, υ, to reconstruct the position of the DT hit:

$$position = (T_{TDC} - T_{ped}) \cdot \upsilon$$

The time pedestal accounts for the time from the bunch crossing until the trigger decision arrives at the chamber electronics.

Hit reconstruction in a CSC layer measures the position of the traversing muon by combining information from the cathode strips and anode wires. The strips are radial and can thus accurately measure the ϕ angle. This is the bending direction of a muon traveling through the endcaps. A CSC hit is reconstructed at the intersection points of hit strips and wire groups.

Hit reconstruction in an RPC chamber requires clustering of hit strips. A charged particle passing through the RPC produces an avalanche of electrons in the gap between the two plates. This charge induces a signal to an external strip readout plane to identify muons from collision events with a precision of a few ns. Since the ionization charge from a muon can be shared by more than one strip, adjacent strips are clustered to reconstruct one hit. An RPC hit is reconstructed as the strip cluster centroid.

While the RPC chambers are single-layer chambers, the CSC and DT are multi-layer detectors where the hits are reconstructed in each layer. From the reconstructed hits, straight-line track "segments" are built within each CSC or DT chamber.

In the standard CMS reconstruction procedure for pp collisions, tracks are first reconstructed independently in the inner tracker and in the muon system, and then used as input for muon track reconstruction.

For the muon component of the CMS trigger, CSC and DT chambers provide "trigger primitives" constructed from hit patterns consistent with muons that originate from the collision region, and RPC chambers provide hit information. The custom-made electronics in the L1 trigger system utilize the chamber information to reconstruct muon trigger candidates with a coarse measurement of p_T. Events selected by the L1 trigger are passes to the HLT, which uses information from the full CMS detector to reconstruct muons.

2.6 Jet reconstruction

Jets are the experimental signatures of quarks and gluons produced in high-energy processes such as head-on pp collisions. As quarks and gluons have a net color charge and cannot exist freely due to color-confinement, they are not directly observed. Instead, they come together to form color-neutral hadrons, a process called hadronisation that leads to a collimated spray of hadrons called a jet.

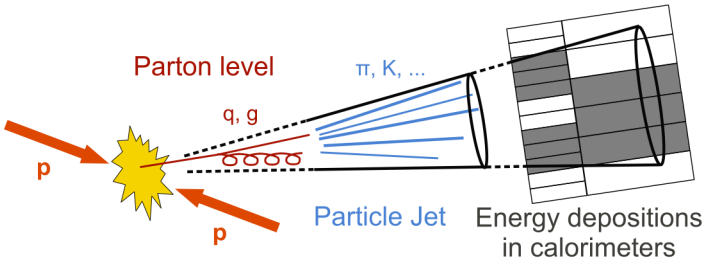

Figure 2.6: Sketch of pp collision and resulting collimated spray of particles, a jet

As these jets of particles propagate through the CMS detector, they leave signals in components such as the tracker, ECAL and HCAL. These signals are combined using jet algorithms to form a reconstructed jet.

Jet reconstruction algorithms are used to combine the calorimetry and tracking information to define jets. The jets provide a link between the observed colorless stable particles and the underlying physics at the partonic level. This link provides information on the kinematics of the originating partons which can be used to shed light on QCD and infer the presence and thus the properties of the Higgs boson and other particles too short lived to be detected.

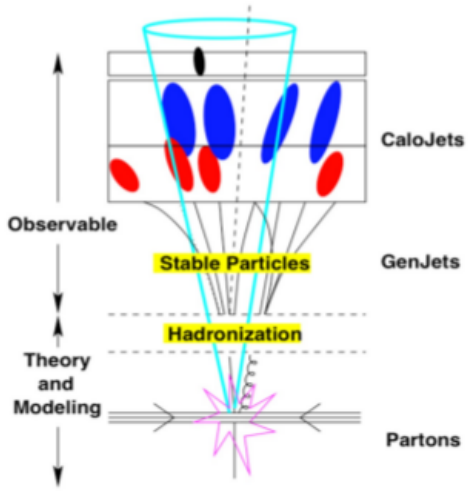

Figure 2.7: A simple example of an event showing the point collision, the fragmentation and hadronization of quarks and gluons and the resulting jet found through the detection of stable particles. Calojets are those jets created using the calorimeter output whereas Genjets are jets created using stable simulated particles. The dashed line represents the direction of the missing energy

A large jet radius is important as it allows the jet to capture enough of the hadronised particles for the accurate calculation of the jets mass and energy. However, a smaller jet radius is useful in reducing the amount of underlying event (UE) and pile-up (PU) captured by the jet, preventing the overestimation of the jet mass and energy.

There are two main classes of jet algorithms in use. The first being the cone algorithms, of which the most important are the iterative cone with progressive removal (IC-PR), the iterative cone with split-merge procedure (IC-SM) and the seedless infrared safe cone (SIScone). The second class is the sequential clustering algorithms which comprises of the K_t, Anti-K_t and the Cambridge/Aachen algorithms.

Cone algorithms assume that particles in jets will show up in conical regions and thus they cluster based on $(\eta - \phi)$ space, resulting in jets with rigid circular boundaries. For example, the IC-PR algorithm is as follows: Find the hardest (largest p_T) cell and make it a seed. Create a cone of radius R around this seed and calculate the trial jet axis by summing up the cells

within this cone using four-vectors. If the trial jet axis is equal to the seed axis, the cone is labelled as stable and all the particles within the stable cone are removed from the list of particles. The next hardest remaining cell is found and this procedure is repeated. But if the trial jet axis does not equal the seed axis, the trial jet axis is made the new seed axis and the process is repeated until convergence of the axes occur. The entire process is repeated until there are no seeds left above a threshold energy.

Sequential clustering algorithms assume that particles within jets will have small differences in transverse momenta and thus groups particles based on momentum space, resulting in jets that have fluctuating areas in $(\eta - \phi)$ space. All sequential clustering algorithms have a similar method. The first distance variable is the one between two particles $d_{ij} = min(p_{Ti}^{\alpha}, p_{Tj}^{\alpha}) \cdot \frac{R_{ij}^2}{R}$, where α is an exponent corresponding to a particular clustering algorithm, $R_{ij}^2 = (\eta_i - \eta_j)^2 + (\phi_i - \phi_j)^2$ is the $(\eta - \phi)$ space distance between the two particles and R is the radius parameter which determines the final size of the jet and is usually between $0.4 - 0.7$. The second distance variable is $d_{iB} = p_{Ti}^{\alpha}$ and is the momentum space distance between the beam axis and the detected particle.

The sequential clustering algorithms work by first finding the minimum of the entire set $\{d_{ij}, d_{iB}\}$. If d_{ij} is the minimum then particles i and j are combined into one particle (ij) using summation of four-vectors after which i and j are removed from the list of particles. If d_{iB} is the minimum, i is labeled as final jet and removed from the list of particles. This process is repeated until either all particles are part of a jet with the distance between the jet axes R_{ij} greater than R, which is inclusive clustering. Or until a desired amount of jets have been found, this is exclusive clustering.

The α value corresponding to the K_t algorithm is 2, resulting in the following equations:

$$d_{ij} = min(p_{Ti}^2, p_{Tj}^2) \cdot \frac{R_{ij}^2}{R}$$
$$d_{iB} = p_{Ti}^2$$

The dominance of low p_T is shown in the first equation and so the K_t algorithm prefers to cluster soft particles first, resulting in an area that fluctuates considerably and an algorithms that is susceptible to the UE and PU. Due to its method of clustering, K_t does a good job at resolving subjets.

The α value corresponding to the Anti-K_t algorithm is -2, resulting in the following equations:

$$d_{ij} = min(\frac{1}{p_{Ti}^2}, \frac{1}{p_{Tj}^2}) \cdot \frac{R_{ij}^2}{R}$$
$$d_{iB} = \frac{1}{p_{Ti}^2}$$

The first equation is dominated by high p_T and the algorithm prefers to cluster hard particles first. Thus the area fluctuates slightly and the algorithm is only slightly susceptible to the UE and PU. The Anti-K_t's clustering preference results in an algorithm that is the best at resolving jets but due to its poor de-clustering, it is the worst for studying jet substructure.

The α value corresponding to the Cambridge/Aachen algorithm is 0, resulting in the following equations:

$$d_{ij} = \frac{R_{ij}^2}{R}$$
$$d_{iB} = 1$$

Both of the distance variables are independent of momentum and so its area fluctuates somewhat and is somewhat susceptible to the UE and PU. Due to the purely spatial character of the distance variables, C/A de-clusters the best and so is the best suited for studying jet substructure. An example of the four main algorithms' jet areas are illustrated below.

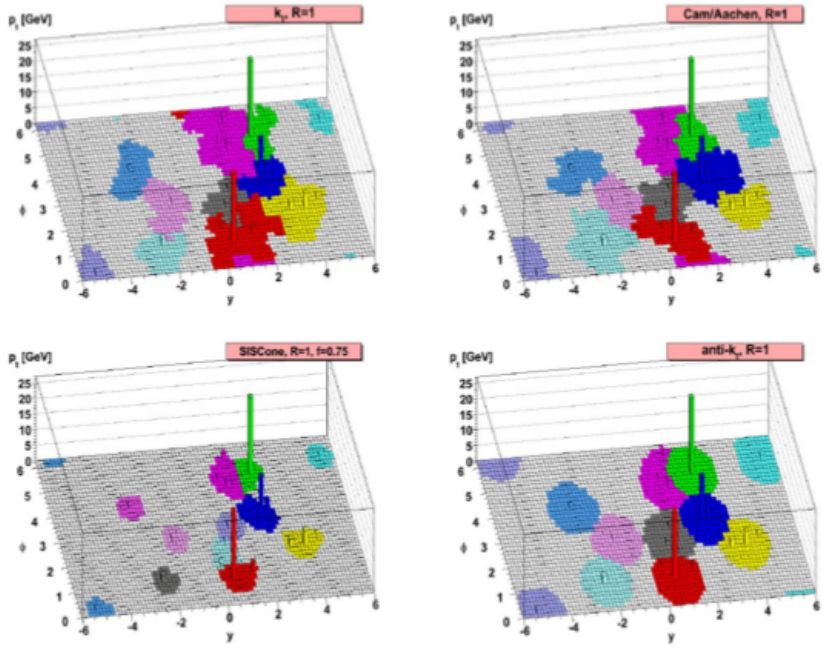

Figure 2.8: The four main jet reconstruction algorithms' areas, performed on the same data with the same input radius. Noted features are the high irregularity in the K_t algorithms area, the conical shape of the Anti-K_t's jets illustrating this algorithms preference for hard radiation and the smaller effective radius of the SIScone, due to the split merge procedure, which can be observed via smaller jet areas and two jets being resolved in the place of just the one grey jet. The different colors are used to represent the different jets and their areas.

In CMS, jets are clustered from the particle flow objects with the Anti-K_t sequential recombination algorithm at a clustering radius of 0.5 (the most accurate jet algorithm for resolving jets is the Anti-K_t algorithm). 65% of the measured jet energy is reconstructed as charged hadrons, 25% as photons, while only the remaining 10% is reconstructed as neutral hadrons. After reconstruction, jets need to be calibrated in order to measure at the same generator jet and reconstructed jet energy scale.

There is a difference between generator jet energy and reconstructed jet energy in simulation resulting from detector simulation effects like nonlinear

calorimeter response, inactive material interactions and physical effects like neutrinos produced in the jet. There are residual differences in jet energy between simulation and data. These residual differences may be caused by time dependent detector response.

The corrections are dependent on a pileup in the event, the angle towards the beampipe (CMS uses the pseudorapidity), and a measure for the energy of the jet (CMS uses the transverse momentum). The CMS collaboration uses factorized correction scheme to calibrate the jet energy scale, first subtracting addinational energy induced by overlaid low-energy pp collisions (pileup) and then correcting for $|\eta|$- and p_T-dependence of the jet energy scale on simulated events. Finally, momentum conserving physics processes are used to measure the jet energy scale on data.

Pileup mitigation. Additional particles coming from secondary interactions, known as pileup (PU), can deteriorate the measurement since they may be clustered in the reconstructed jets. The CMS collaboration uses a variety of techniques for PU mitigation. One example is the Charged Hadron Subtraction (CHS) algorithm. It uses the information from the tracker to remove the charged particles that are associated with a pileup vertex from the jet clustering procedure. Due to its limited coverage in η, outside the tracker no information on the charge of a particle is available; consequently, dedicated jet energy corrections are applied to account for the impact of charged PU outside the tracker coverage, and of neutral PU everywhere. This approach is limited since the additional corrections act on the four-momentum and not on the jet shape or substructure. To overcome this limitation, an alternative technique for PU mitigation, pileup per particle identification (PUPPI), is introduced. It calculates, event by event, a probability that each particle originates from the leading primary vertex and scales the energy of these particles based on that probability.

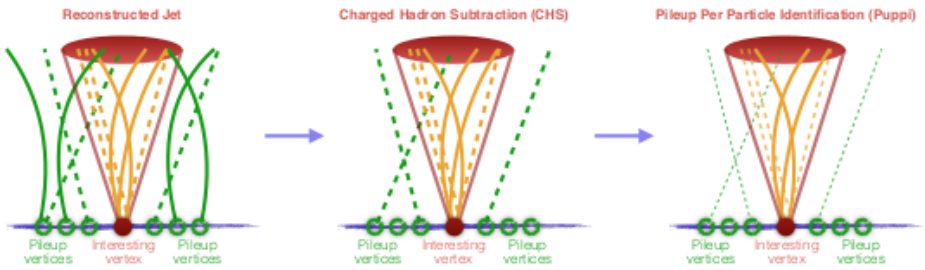

Figure 2.9: Sketch of PU suppression techniques

2.7 b-tagging

The hadronization of a b quark produces a B hadron which propagates a measurable distance before decaying. Such behavior leads to special properties of the arising b jet, like the presence of an inner displaced secondary vertex with a flying distance higher than its resolution. Tracks coming from a secondary vertex have a large impact parameter that can also be used to identify b jets. Besides, in 20% of cases, a b jet will contain a lepton coming from the semi-leptonic decay of the B hadron. These features are used to build taggers, yielding a single discriminator value for each jet.

The b-tagging algorithm and their study are based on the measure of three main variables: the impact parameter significance of the tracks, the position of the secondary vertex, and the transverse momentum of the muon relative to the jet direction.

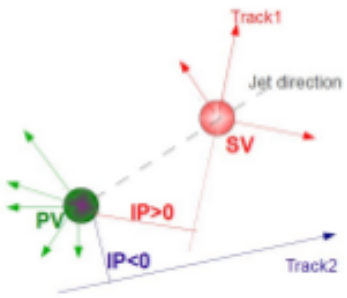

Figure 2.10: Geometric meaning of the impact parameter significance

The impact parameter (IP) is defined as the distance between the track and the primary interaction vertex (PV) at the point of closest approach. The IP is positive (negative) if the track is produced downstream (upstream) with respect to the PV along the jet direction. In practice, the impact parameter significance IP/σ(IP) is used in order to take into account resolution effects. The secondary vertex is the point where the B hadron decays.

The output of each b-tagging algorithm is a discriminator value on which one can cut more or less tightly, in order to distinguish b-jets from non-b jets.

- The **Track Counting** algorithm identifies a b-jet if there are at least N tracks with a significance of the impact parameter above a given threshold. The tracks are organized in decreasing IP/σ(IP) and the discriminator is the impact parameter significance of the Nth track. This is a very simple tag, exploiting the long lifetime of B hadrons. It comes in two variations for N = 2 (high efficiency) or N= 3 (high purity).

- The **Jet Probability** algorithm relies on the IP/σ(IP) measurement of all tracks in a jet. One can use the negative tail of the IP/σ(IP) distribution to extract the probability density function for tracks not coming from b/c-jets. By integrating on the PDF, we can compute the

probability for tracks to originate from the PV. Then combining the probability of the tracks we can assign to the jet a probability to come from the PV. Its b tag discriminator is equal to the negative logarithm of the confidence level that all the tracks in the jet are consistent with originating from the PV.

- **Soft-Lepton** tagging algorithms rely on the properties of muons or electrons from semileptonic b-decay. Due to the large b-quark mass, the momentum of the muon transverse to the jet axis is larger for muons from B-hadron decays than for muon in light flavor jets.

- **Secondary Vertex** tagging algorithms rely on the reconstruction of at least one secondary vertex. The significance of the 3D flight is used as a discriminating variable. Reconstructs the B decay vertex using an adaptive vertex finder, and then uses variables related to it, such as decay length significance to calculate its b tag discriminator.

- The **Combined Secondary Vertex** algorithm is a complex tag and exploits all known variables, which can distinguish b from non-b jets. It provides optimal b tag performance, by combining information about impact parameter significance, the secondary vertex and jet kinematics.

2.8 Particle Flow Algorithm

The Particle Flow (PF) algorithm aims at identifying and reconstructing all the particles from the collision by combining optimally the information of the different subdetectors. The CMS PF algorithm relies on a efficient and pure track reconstruction, on a clustering algorithm able to disentangle overlapping showers, and on an efficient link procedure to connect together the deposits of each particle in the subdetectors. The tracks are extrapolated through the calorimeters, if they fall within boundaries of one or several clusters, the clusters are associated to the track. The set of track and cluster constitute a charged hadron. The muons are identified beforehand so that their track does not give rise to a charged hadron. For the electrons, due to

the frequent Bremsstrahlung photon emission, a specific track reconstruction is needed as well as a dedicated treatment to properly attach the photon clusters to the electron. Once all tracks are treated, the remaining clusters result in photon in case of ECAL and neutral hadrons in the HCAL. The resulting list of particles, namely charged hadrons, photons, neutral hadrons, electrons and muons, is then used to reconstruct the jets, the missing transverse energy and the taus from their decay products.

The figure below shows a jet simulated in the CMS detector with $p_T = 65$ GeV. This jet is made of only five particles for illustrative purposes: two charged hadrons (π^+, π^-), two photons (from the decay of a π^0) and one neutral hadron (K_L^0). The charged hadron tracks are identified by a geometrical connection in the (η, ϕ) views between one track and one or more calorimeter clusters, and by the absence of signal in the muon detectors. The photons and neutral hadrons are in general identified by ECAL and HCAL clusters respectively with no track link. No attempt is made to distinguish the various species of neutral and charged hadrons in the PF reconstruction. Electrons would be identified by a track and an ECAL cluster, while muons by a track in the inner tracker connected to a track in the muon detectors.

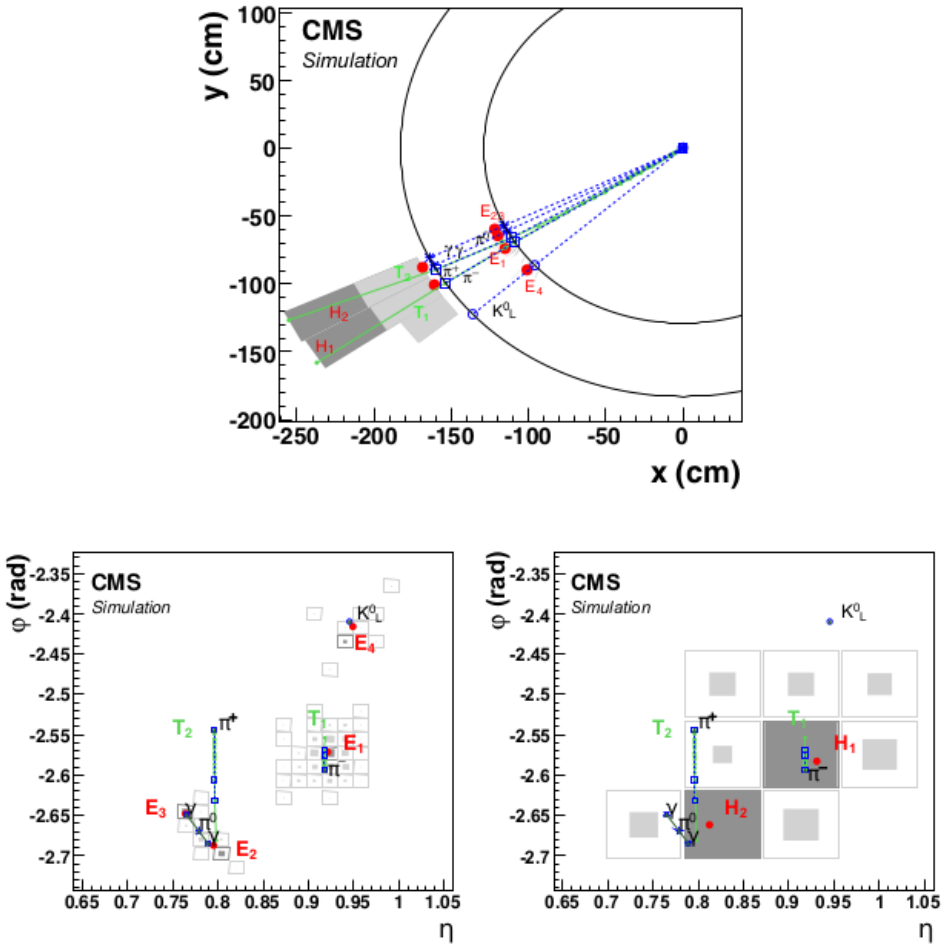

Figure 2.11: Event display of a jet in the (x,y) view (upper panel) and in the (η, ϕ) view on ECAL surface (lower left) and the HCAL surface (lower right). In the top view, these two surfaces are represented as circles centered around the interaction point. The K^0_L, the π^-, and the two photons are detected as four well-separated ECAL clusters denoted $E_{1,2,3,4}$. The π^+ does not create a cluster in the ECAL. The two charged pions are reconstructed as charged particle tracks $T_{1,2}$. These tracks point towards two HCAL clusters $H_{1,2}$. In the bottom views, the ECAL and HCAL cells are represented as squares, with an inner area proportional to the logarithm of the cell energy. Cells with an energy larger than those of the neighbouring cells are shown in dark gray.

2.9 Monte Carlo Generators

In real life, machines produce events that are stored by the data acquisition system of a detector. In the virtual reality, event generators like HERWIG and PYTHIA play the role of machines like the LHC, and detector simulation programs like GEANT the role of detectors like CMS. The real and virtual worlds can share the same event reconstruction framework and subsequent physics analysis. It is by understanding how an original physics input is distorted step by step in the better controlled virtual world that an understanding can be gained of what may be going on in the real world.

In quantum mechanics, calculations provide the probability for different outcomes of a measurement. Event by event, it is impossible to know beforehand what will happen: anything that is at all allowed could be next. It is only when averaging over large event samples that the expected probability distributions emerge. In generators, pseudorandom numbers are used to make choices intended to reproduce the quantum mechanical probabilities for different outcomes at various stages of the process.

The general idea is "instead of performing long complex calculations, perform large number of experiments using random number generation and see what happens". Monte Carlo assumes the system is described by probability density functions which can be modeled. Particle physics uses MC for detector design and optimization, simulation of particle interactions with detector's material.

In HEP we use two types of MC methods: MC for event generation and calculation of process cross section and MC simulation of detectors.

The structure of pp collisions at the LHC as built up by event generators can be described by a few main steps. These are illustrated in the figure below where two protons come in from either side and make a collision. The color coding corresponds to the steps into which most event generators divide the process:

1. Hard process
2. Parton shower
3. Hadronization
4. Underlying event

5. Unstable particle decays

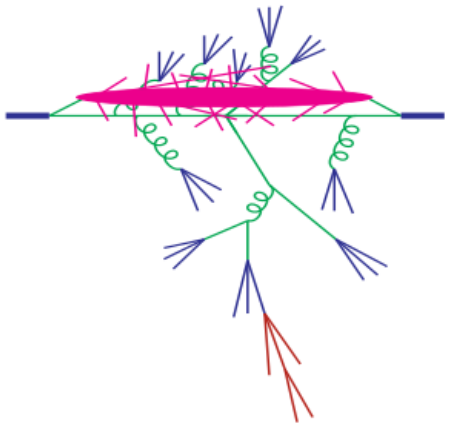

Figure 2.12: Diagram showing the structure of pp collision, where the different colors indicate the different stages involved in event generation

The first thing an experimentalist notices when studying pp collisions is that most of them are "boring" in the sense that only a few soft hadrons are produced and most of the event goes out along the beam pipe direction. Only a tiny fraction of events contain a high momentum-transfer process of interest. It is therefore not feasible to simulate all possible pp collisions but the simulation needs to be structured with a focus on deciding what hard process is wanted (a bit like triggers at experiments which decide which events to write to tape and which to discard).

This is done by starting the simulation at the heart of the collision and calculating from perturbation theory the probability distribution of a particular hard scatter, which is the highest momentum transfer process in the event. Simulating the hard process is relatively straightforward because the parton distribution functions describe partons coming into the process and lowest order perturbation theory gives a probabilistic distribution of the outgoing partons.

A more interesting stage of event generation comes from asking what happens to the incoming and outgoing partons involved in the hard collision. This is described by the parton shower phase of event generators. The partons involved in the hard process are colored particles, quarks and gluons. From QED it is well known that scattered electric charges radiate photons,

this is what is called Bremsstrahlung. In the same way, scattered colored charges radiate gluons and this happens for partons on their way in and out of a collision. The main difference to QED is that, due to the non-Abelian structure of $SU(3)$, gluons themselves are colored and so an emitted gluon can itself trigger new radiation. This leads to an extended shower and the phase space fills up with mostly soft gluons. The parton shower can be simulated as a sequential step-by-step process that is formulated as an evolution in momentum transfer scale. The parton shower evolution starts from the hard process and works downwards to lower and lower momentum scales to a point where perturbation theory breaks down.

Here it is necessary to switch to hadronization models, which take account of the confinement of a system of partons into hadrons, which are seen in the detector. As well as the confinement of the produced partons, it is important to remember that the initial, uncolored proton has had a colored parton taken out if it and so it has been left in colored state. To get an idea of the space time structure of a collision, consider the fact that in a proton's won rest frame it is a spherical bound state, but in the lab frame the two protons are moving towards each other at very high speed and the Lorentz contraction flattens them into extremely tiny pancakes. The collision happens at a point where these flat discs are completely overlapping each other in space and so there is a very high probability that there will be other interactions apart from the hard interaction. This gives rise to the underlying event, which is made up of secondary interactions between proton remnants. It produces soft hadrons everywhere in the event, which overlie and contaminate the hard process that was already simulated.

The last component of event generation is the fact that many of these hadrons are not stable particles but heavy resonances that then go on to decay.

Analysis

3.1 Signal and Background events

In this analysis, we present a search for an excited bottom quark which decays into a top quark and a W boson, where the W boson decays leptonically and reconstructed as a lepton (μ) and a missing transverse energy, while the top quark decays hadronically and reconstructed as a jet identified as originating from a bottom quark and as two jets with invariant mass equal to the W boson mass. A Feynman diagram of the signal event we are searching for is shown below.

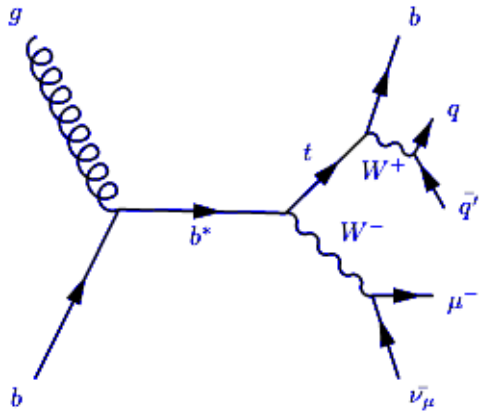

Figure 3.1: Signal event

A b^* can be produced from a gluon and a bottom quark via the strong interaction, as described by the effective Lagrangian:

$$\mathcal{L} = \frac{g_s}{2\Lambda} G_{\mu\nu} \bar{b} \sigma^{\mu\nu} (\kappa_L^b P_L + \kappa_R^b P_R) b^* + h.c$$

In this formula, g_s is the strong coupling, $G_{\mu\nu}$ is the gauge field tensor of the gluon, Λ is the scale of the new physics, which is chosen to be the mass of b^*, P_L and P_R are the chiral projection operators, κ_L^b and κ_R^b are the corresponding relative coupling strengths.

The decay of b^* in this analysis proceeds through the weak interaction as is described by the Lagrangian:

$$\mathcal{L} = \frac{g_2}{\sqrt{2}} W_\mu^+ \bar{t} \gamma^\mu (g_L P_L + g_R P_R) b^* + h.c$$

where g_2 is the weak coupling, g_L and g_R are the relative coupling strength to the left-handed and right-handed b^*.

The benchmark cases considered are a purely left-handed b^* quark with $g_L = 1, \kappa_L^b = 1, g_R = 0, \kappa_R^b = 1$.

The search strategy consist of a bump hunting in the top and the leptonically decaying W boson invariant mass spectrum. Models with excited bottom quarks of different masses had been compared against the background-only model, but the models with signal do not reproduce the data significantly better than the background alone. Therefore, we instead set a limit on our sensitivity to detect excited bottom quarks below a certain mass.

Events that highly resemble the signal event final state are considered backgrounds to the signal. In our analysis, the background events are the single top production in the t-channel, $t\bar{t}$ production where one b quark from the t or $\bar{t}$ decay has not been detected, the Drell-Yann+Jets where the one muon from the Z boson decay has not been detected and the one b quark from the gluon decay has not been identified as b (tagging algorithms are not perfect, rather they are coming with an identification efficiency and a probability to misidentify), and the W+Jets where again one of the b quarks from the gluon decay has been misidentified. Feynman diagrams of the background events are shown below:

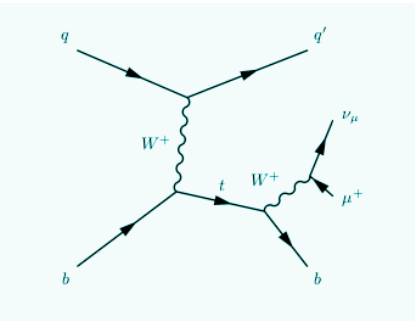

(a) single top t-channel

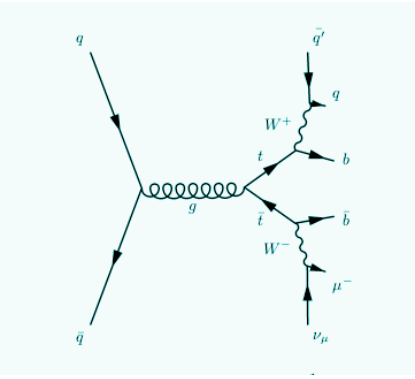

(b) $t\bar{t}$

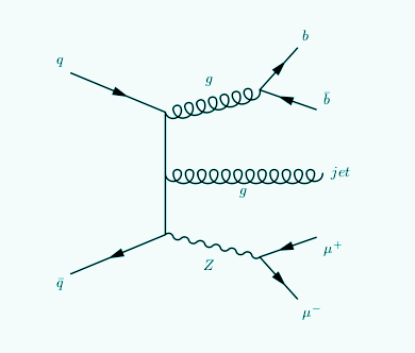

(c) Drell-Yann+Jets

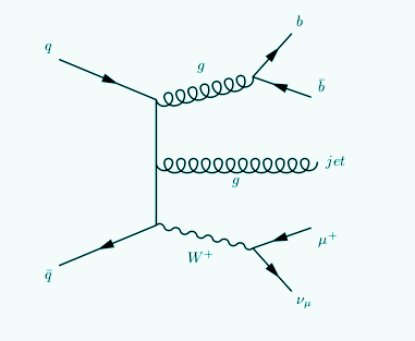

(d) W+Jets

Figure 3.2: Background events

b^* simulated samples for left-handed chiralities are generated, starting from b^* mass 1200 GeV and up to 2400 GeV in steps of 200 GeV. The table below summarizes the product of cross section and branching ratio to tW of these signal samples. b^* samples are generated with MADGRAPH, showered by PYTHIA with tune CUETP8M1.

chirality-mass[GeV]	cross-section[pb]
LH-1200	1.98
LH-1400	0.81
LH-1600	0.35
LH-1800	0.17
LH-2000	0.081
LH-2200	0.041
LH-2400	0.022

The background Monte Carlo samples and its production cross sections used are listed in the table below. The single top t-channel and $t\bar{t}$ backgrounds are simulated with POWHEG matrix element generator, while the WJets and DYJets backgrounds with MADGRAPH.

process	cross section [pb]
flatTree_ST_t-channel_top_4f_inclusiveDecays_13TeV-powhegV2-madspin-pythia8_TuneCUETP8M1	136.02
flatTree_ST_t-channel_antitop_4f_inclusiveDecays_13TeV-powhegV2-madspin-pythia8_TuneCUETP8M1	80.95
flatTree_TT_TuneCUEPT8M2T4˙13TeV-powheg-pythia8	832
flatTree_WJetsToLNu_HT-70to100_TuneCUETP8M1_13TeV-madgraphMLM-pythia8	1353
flatTree_WJetsToLNu_HT-100to200_TuneCUETP8M1_13TeV-madgraphMLM-pythia8	1346
flatTree_WJetsToLNu_HT-200to400_TuneCUETP8M1_13TeV-madgraphMLM-pythia8	359.7
flatTree_WJetsToLNu_HT-400to600_TuneCUETP8M1_13TeV-madgraphMLM-pythia8	48.91
flatTree_WJetsToLNu_HT-600to800_TuneCUETP8M1_13TeV-madgraphMLM-pythia8	12.05
flatTree_WJetsToLNu_HT-800to1200_TuneCUETP8M1_13TeV-madgraphMLM-pythia8	5.501
flatTree_WJetsToLNu_HT-1200to2500_TuneCUETP8M1_13TeV-madgraphMLM-pythia8	1.329
flatTree_WJetsToLNu_HT-2500toInf_TuneCUETP8M1_13TeV-madgraphMLM-pythia8	0.03216
flatTree_DYJetsToLL_M-50_HT-70to100_TuneCUETP8M1_13TeV-madgraphMLM-pythia8	169.9
flatTree_DYJetsToLL_M-50_HT-100to200_TuneCUETP8M1_13TeV-madgraphMLM-pythia8	147.4
flatTree_DYJetsToLL_M-50_HT-200to400_TuneCUETP8M1_13TeV-madgraphMLM-pythia8	40.99
flatTree_DYJetsToLL_M-50_HT-400to600_TuneCUETP8M1_13TeV-madgraphMLM-pythia8	5.678
flatTree_DYJetsToLL_M-50_HT-600to800_TuneCUETP8M1_13TeV-madgraphMLM-pythia8	1.367
flatTree_DYJetsToLL_M-50_HT-800to1200_TuneCUETP8M1_13TeV-madgraphMLM-pythia8	0.6304
flatTree_DYJetsToLL_M-50_HT-1200to2500_TuneCUETP8M1_13TeV-madgraphMLM-pythia8	0.1514
flatTree_DYJetsToLL_M-50_HT-2500toInf_TuneCUETP8M1_13TeV-madgraphMLM-pythia8	0.003565

Each process has to be scaled to its expected number of events which is given as a product of the acceptance in Monte Carlo, the cross section of the process and the luminosity ($L = 36.3$ fb^{-1}):

$$N_{exp} = (\text{acceptance in MC}) \cdot \sigma \cdot L$$

where the acceptance in Monte Carlo is defined as the fraction of the total generated Monte Carlo events that pass all the cuts, that is

$$(\text{acceptance in MC}) = \frac{N_{ent}}{N_{tot}^{MC}}$$

where N_{tot}^{MC} are the total generated Monte Carlo events and N_{ent}^{hist} are the number of events from the total generated Monte Carlo that survive our analysis cuts.

After scaling each process, we consider the single top and antitop production processes as one by simply adding them, similarly we add the W+Jets processes with different transverse energy (H_T) ranges $\{(70, 100), (100, 200), (200, 400), (400, 600), (600, 800), (800, 1200), (1200, 2500), (2500, \infty)\}$ and consider them as one, as well as for the Drell-Yann+Jets processes. Thus, we end up with four different background processes.

In order to obtain the desired signal final state we have to apply some baseline selection criteria, widely known as preselection "cuts":

- at least 3 jets one of which is b-tagged
- exactly one muon (muon or anti-muon)

To reconstruct the hadronically decaying W boson, from the set of jets we are choosing those two non-b jets which give the smallest invariant mass. To further reduce the background we can apply extra cuts on the kinematic variables of the objects used in the analysis:

- MET > 40 GeV
- $p_{T,muon} > 100$ GeV

- for all jets $|\eta_{jet}|< 3$
- for all jets $p_{T,jet} < 350$ GeV
- invariant mass of hadronically decaying W: 50 GeV $< m_W <$ 120 GeV
- $\Delta R_{b,muon} = \sqrt{(\eta_b - \eta_{muon})^2 + (\phi_b - \phi_{muon})^2} > 2$
- invariant mass of b jet, muon and neutrino: $m_{b,muon,\nu} > 350$ GeV
- invariant mass of top: 160 GeV $< m_t <$ 230 GeV
- $\Delta R_{t,W} = \sqrt{(\eta_t - \eta_W)^2 + (\phi_t - \phi_W)^2} > 3$

The variables MET and $p_{T,muon}$ are not independent since there is a constraint on their four momenta: $(p_\nu + p_{muon})^2 = m_W^2$, where at first approximation $p_{T,\nu}$ = MET. To find the best cut for the transverse momentum of the muon, $p_{T,muon}$, we calculate the quantity

$$F = \frac{S}{\sqrt{B+S}}$$

called figure of merit, within a mass window of the excited b quark [1000 GeV,1500 GeV], for different cut values on $p_{T,muon}$. S and B are the signal and background yields respectively. The maximum value of F corresponds to the best cut on $p_{T,muon}$. Assuming that the variables S and B are independent, the error on the quantity F is given by

$$\begin{aligned}
\delta F &= \sqrt{(\frac{\partial F}{\partial S}\delta S)^2 + (\frac{\partial F}{\partial B}\delta B)^2} \\
&= \sqrt{(\frac{1}{\sqrt{B+S}} + (-\frac{1}{2})\frac{S}{(B+S)^{3/2}})^2\delta S^2 + ((-\frac{1}{2})\frac{S}{(B+S)^{3/2}})^2\delta B^2} \\
&= \sqrt{\frac{(B+S/2)^2\delta S^2 + (S/2)^2\delta B^2}{(B+S)^3}}
\end{aligned}$$

Since

$$S = \frac{\sigma_{sig} L N_{ent,sig}}{N^{MC}_{tot,sig}}$$
$$B = \frac{\sigma_{bkg} L N_{ent,bkg}}{N^{MC}_{tot,bkg}}$$

the uncertainties for the signal and background yields are

$$\delta S = \frac{\sigma_{sig} L \sqrt{N_{ent,sig}}}{N^{MC}_{tot,sig}}$$
$$\delta B = \frac{\sigma_{bkg} L \sqrt{N_{ent,bkg}}}{N^{MC}_{tot,bkg}}$$

Jets are reconstructed using information from the calorimeters and the tracker. Since the pseudorapidity coverage of the ECAL and the HCAL is $|\eta| < 3$, we want our jets to have absolute value of pseudorapidity smaller than 3.

We can construct a two dimensional scatter plot of the jets transverse momentum versus the jets mass. We notice that there are jets with $p_T > 350$ GeV which has mass around the W boson mass (80 GeV). These jets are originating from a high p_T W boson and are overlapped and regarded as one. Since we are not concerned with boosted topology, we are selecting jets with transverse momentum lower than 350 GeV.

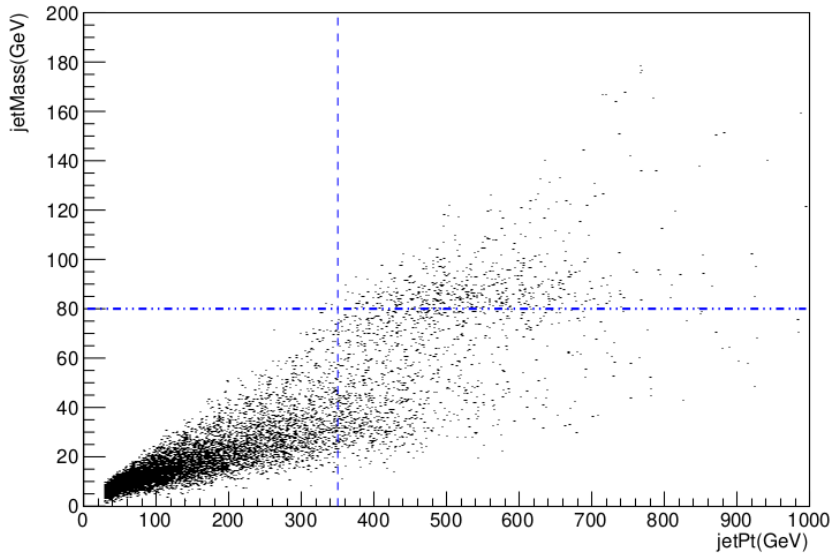

Figure 3.3: A scatter plot of jet p_T versus jet mass showing our choice of cut on the $p_{T,jet}$ to be 350 GeV

Choosing a narrow window around the mass of the hadronically decaying W and the mass of the top quark considerably reduces the background. We chose the windows in such a way that the reduction of the background being the largest possible while the reduction of the signal being the smallest possible. Furthermore, we would like the t and W to which the excited bottom quark decays to be produced back-to-back, therefore we require $\Delta R_{t,W} > 3$.

To explicitly state that we are interested in the signal event (a) of the figure below and not in the "flipped signal" event (b), we require that the muon and the b jet from the top quark decay to be far enough, that is the objects muon and b jet are both not coming from the top decay, and the invariant mass of the objects muon, b jet and neutrino does not gives us the invariant mass of the top. These requirements are done with the cuts $\Delta R_{b,muon} > 2$ and $m_{b,muon,n} > 350$ GeV respectively.

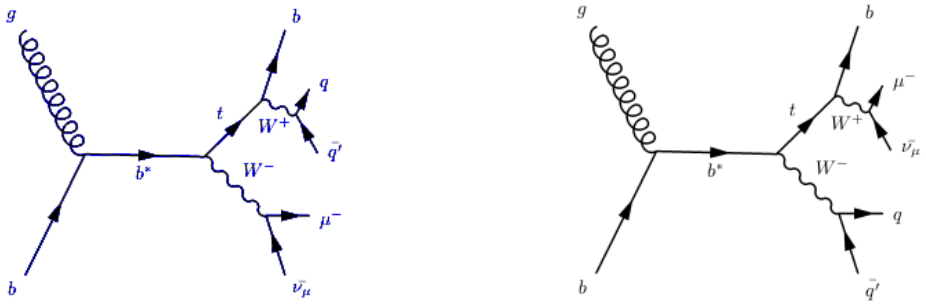

(a) $b^* \to t(bq\bar{q}')W(\mu\nu_\mu)$ (b) $b^* \to t(b\mu\nu_\mu)W(q\bar{q}')$

Figure 3.4: Signal event (a) and "flipped signal" event (b)

After applying all the cuts the expected number of events for each process is

process	N_{exp}
ST	19.9833
TT	4063.52
DYJets	40.0514
WJets	405.828
signal ($m_{b^*} = 1200$ GeV)	188.31
signal ($m_{b^*} = 1400$ GeV)	55.5717
signal ($m_{b^*} = 1600$ GeV)	17.787
signal ($m_{b^*} = 1800$ Gev)	8.57769
signal ($m_{b^*} = 2000$ GeV)	2.88149
signal ($m_{b^*} = 2200$ GeV)	1.45761
signal ($m_{b^*} = 2400$ GeV)	0.710754

The transverse momentum distribution of muons and jets as well as the distribution of missing transverse energy for all processes considered with the signal mass being 1200 GeV are shown in the figures below as stack histograms (first the background process with the smallest expected number of events is drawn (ST), upon it the sum of background processes with the smallest and the next smallest expected number of events is drawn (ST+DYJets)

and so on. The signal process is simply drawn on the same plot and not as stack).

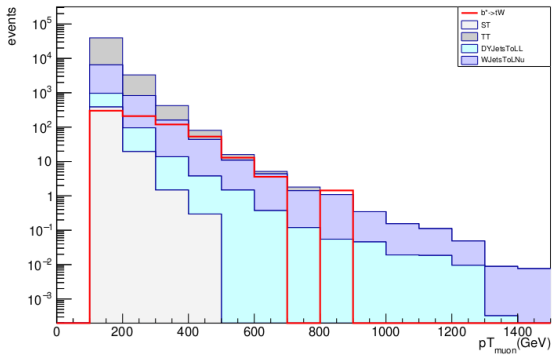

(a) Transverse momentum distribution of muons

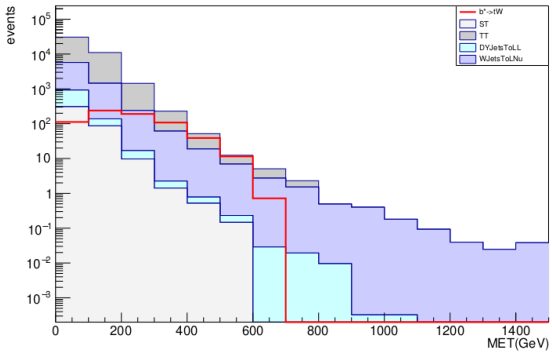

(b) Distribution of MET

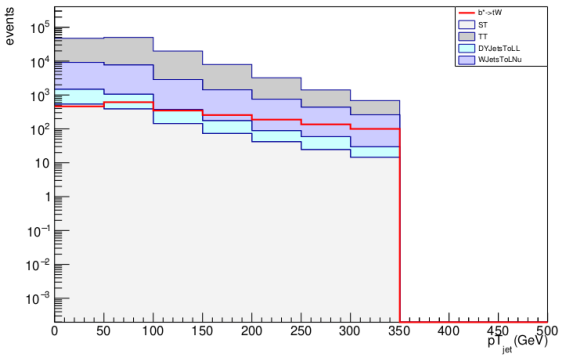

(c) Transverse momentum distribution of jets

Figure 3.5: Stacked histograms of transverse momentum of muons (a), of missing transverse energy, MET (b), and of transverse momentum of jets (c)

Below the pseudorapidity and the ϕ angle distributions of muons and jets are shown. To reconstruct muons we need information both from the tracker and the muon chambers. Since the tracker pseudorapidity coverage is $|\eta|< 2.4$, muons only within that pseudorapidity range can be reconstructed. The ϕ distributions of muons and jets are uniform in the range $(-\pi, \pi)$, which means that the collision products have equal probability to be produced in

any direction on a plane transverse to the beam pipe.

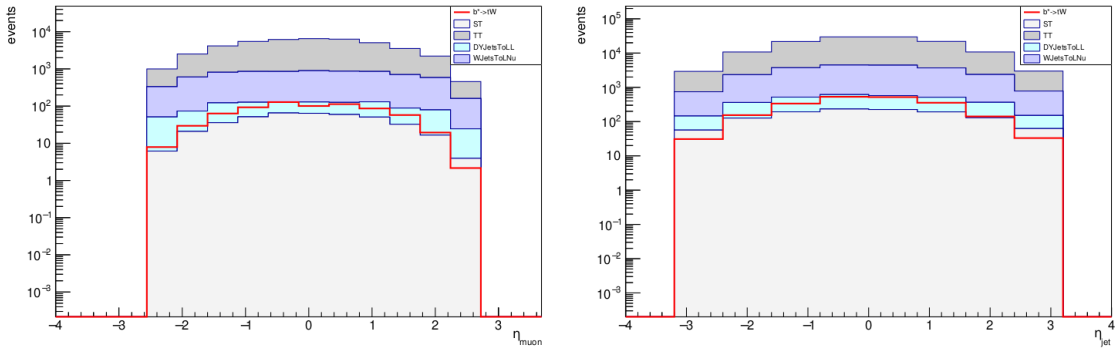

(a) Pseudorapidity distribution of muons

(b) Pseudorapidity distributions of jets

Figure 3.6: Pseudorapidity distributions of muons (a) and jets (b)

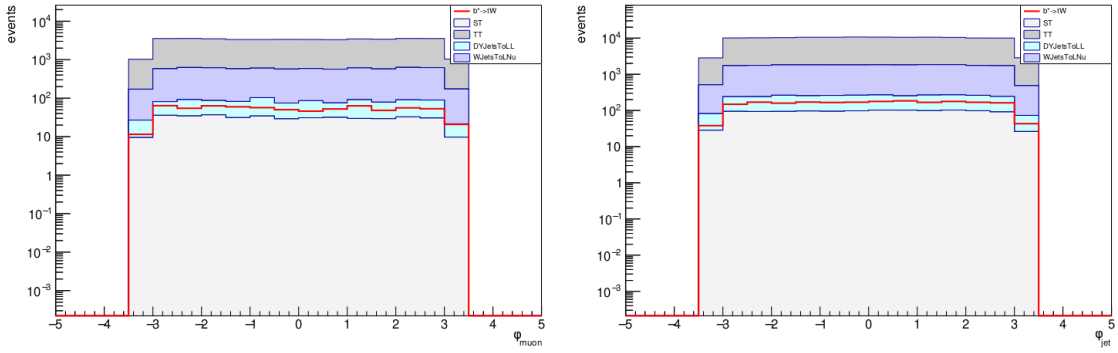

(a) ϕ distribution of muons

(b) ϕ distributions of jets

Figure 3.7: ϕ distributions of muons (a) and jets (b)

We have a W boson which decays hadronically (to a quark and an anti-quark of a different flavor) and a top quark which decays to a b quark and to a hadronic W boson. Their invariant mass is computed from

$$m_W^2 = (p_q + p_{\bar{q}'})^2$$
$$m_{top}^2 = (p_b + p_W)^2$$

and distributions of them are shown in the figure below.

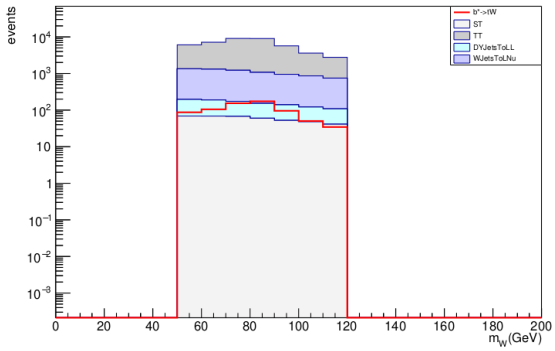

(a) Invariant mass of hadronically decaying W

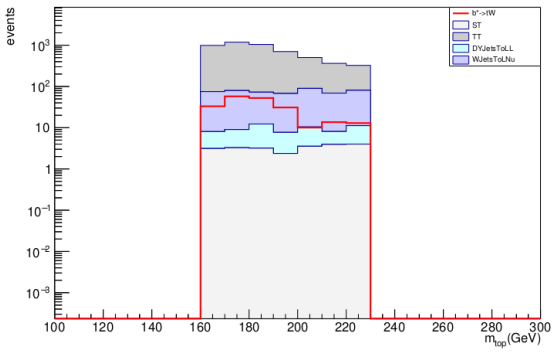

(b) Invariant mass of top quark

Figure 3.8: Invariant masses of hadronically decaying W boson (a) and top quark (b)

3.2 Neutrino reconstruction

Assuming that the W boson was produced on the mass shell, it is possible to infer the z-component of the neutrino momentum from the conservation of four-momentum:

$$\begin{aligned} m_W^2 &= (p_l + p_\nu)^2 \\ &= p_l^2 + p_\nu^2 + 2p_l p_\nu \\ &\approx 2p_l p_\nu \\ &= 2E_l E_\nu - 2\vec{p_l} \cdot \vec{p}_\nu \\ &\approx 2p_l \sqrt{p_{\nu T}^2 + p_{\nu z}^2} - 2(\vec{p}_{lT} \cdot \vec{p}_{\nu T} + p_{lz} p_{\nu z}) \end{aligned}$$

Rearranging terms and taking the square we have a quadratic equation in $p_{\nu z}$

$$p_{lT}^2 p_{\nu z}^2 + [\ -2p_{lz}(\frac{m_W^2}{2} + \vec{p}_{lT} \cdot \vec{p}_{\nu T})]\ p_{\nu z} + [\ p_l^2 p_{\nu T}^2 - (\frac{m_W^2}{2} + \vec{p}_{lT} \cdot \vec{p}_{\nu T})^2]\ = 0$$

The determinant is

$$\Delta = 4p_l^2[\ (\frac{m_W^2}{2} + \vec{p}_{lT} \cdot \vec{p}_{\nu T})^2 - p_{lT}^2 p_{\nu T}^2]$$

If $\Delta > 0$ we have two solutions and we are choosing the lowest $p_{\nu z}$. The case $\Delta = 0$ never happens in practice. The case $\Delta < 0$ corresponds to unphysical solutions, and we cannot just ignore them. For example, for the signal process with an assumed mass of 1200 GeV approximately 70% of the events have $\Delta > 0$ while approximately 30% of the events have $\Delta < 0$, as shown on the plot below.

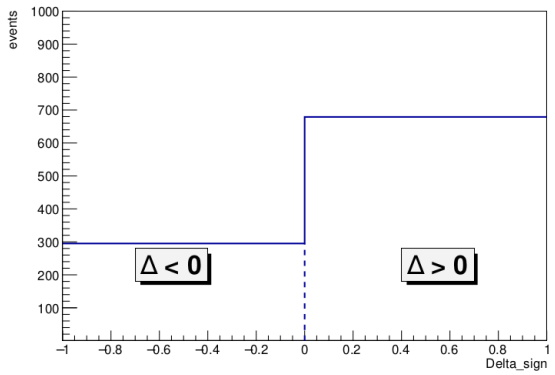

Figure 3.9: Sign of the determinant for the signal process with $m_{b^*} = 1200$ GeV

The way we treat it is to reevaluate our first estimation, $MET(x, y) = (p_{\nu x}, p_{\nu y})$, and say that since the objects went undetected could be jets too, the MET that we have assigned only to neutrinos involves more information, so we have to scale down $p_{\nu x}, p_{\nu y}$ so that

$$\Delta = 0$$
$$(\frac{m_W^2}{2} + \vec{p}_{lT} \cdot \vec{p}_{\nu T})^2 - p_{lT}^2 p_{\nu T}^2 = 0$$

This leads to a quadratic equation in $p_{\nu y}$:

$$-p_{lx}^2 p_{\nu y}^2 + (m_W^2 + 2p_{lx}p_{\nu x})p_{ly}p_{\nu y} + (\frac{m_W^4}{4} + m_W^2 p_{lx}p_{\nu x} - p_{ly}^2 p_{\nu x}^2) = 0$$

Taking the case where the determinant of the last equation is greater than zero, we have two families of solutions:

$$p_{\nu y1} = \frac{p_{ly}}{2p_{lx}^2}(m_W^2 + 2p_{lx}p_{\nu x}) - \frac{m_W p_{lT}}{2p_{lx}^2}\sqrt{m_W^2 + 4p_{lx}p_{\nu x}}$$
$$p_{\nu y2} = \frac{p_{ly}}{2p_{lx}^2}(m_W^2 + 2p_{lx}p_{\nu x}) + \frac{m_W p_{lT}}{2p_{lx}^2}\sqrt{m_W^2 + 4p_{lx}p_{\nu x}}$$

By iterating $p_{\nu x}$ in the range $(p_{\nu x,min}, p_{\nu x,max})$ with step 1 GeV we are creating a lot of candidates $(p_{\nu x}, p_{\nu y1})$, $(p_{\nu x}, p_{\nu y2})$ for the new transverse momentum of the neutrino. From all those, we are choosing the one which is closest to the initial MET.

By construction the invariant mass of the W boson which decays leptonically is a delta function at the mass of the W. This is shown below.

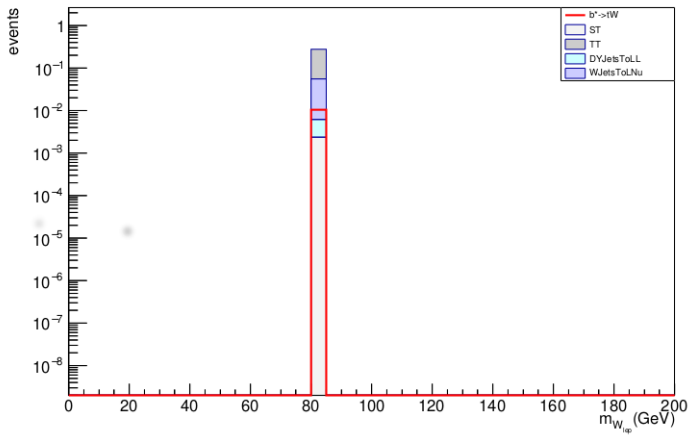

Figure 3.10: Invariant mass of leptonically decaying W boson

After reconstructing the neutrino we are able to reconstruct the excited b quark (b^*) from its decay products ($b^* \to t + W(\mu\bar{\nu}_\mu), t \to b + W(q\bar{q'})$ and from four momentum conservation principle:

$$\begin{aligned} m_{b^*}^2 &= (p_{top} + p_{W_{lep}})^2 \\ &= (p_\mu + p_{\bar{\nu}_\mu} + p_b + p_q + p_{\bar{q'}})^2 \end{aligned}$$

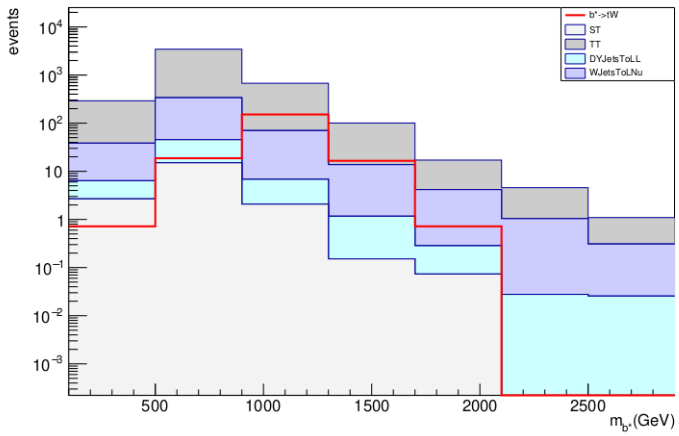

Figure 3.11: Invariant mass of the excited b quark with $m_{b^*} = 1200$ GeV

In the figures below the invariant mass of the excited b quark is shown for different mass hypotheses.

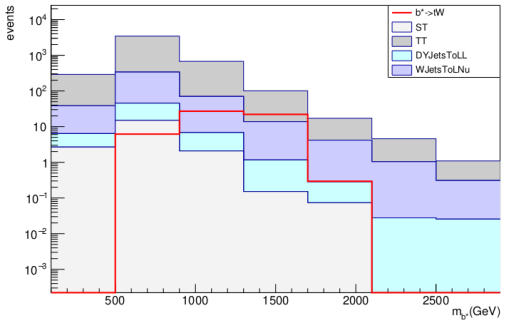

(a) $m_{b^*} = 1400$ GeV

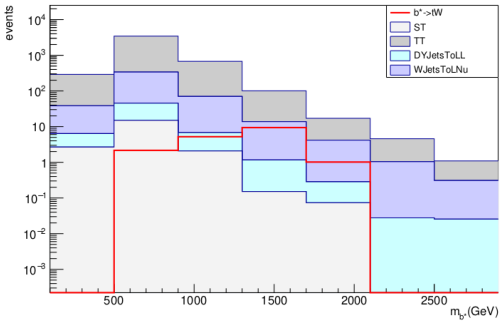

(b) $m_{b^*} = 1600$ GeV

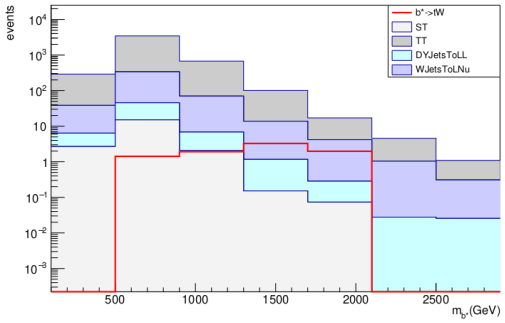

(c) $m_{b^*} = 1800$ GeV

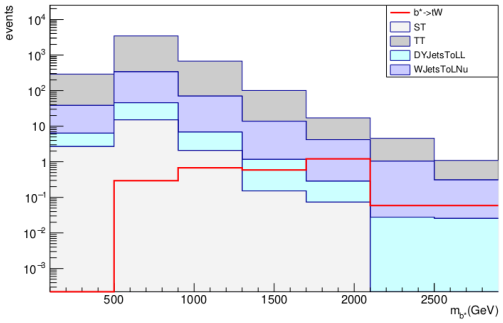

(d) $m_{b^*} = 2000$ GeV

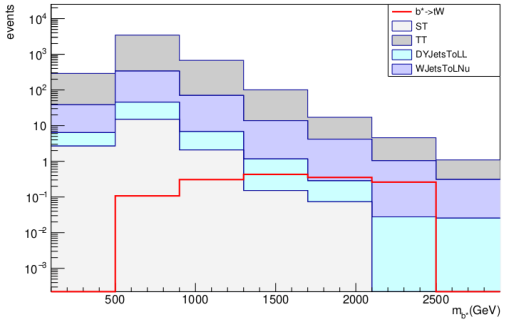

(e) $m_{b^*} = 2200$ GeV

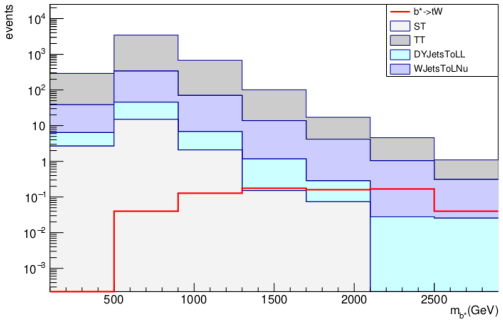

(f) $m_{b^*} = 2400$ GeV

Figure 3.12: Distributions of the invariant mass of the excited b quark for different mass hypotheses

3.3 CLs method - cross section upper limit setting

Suppose that the probability density function of the random variable m_{b^*} for the signal process is $F_{signal}(m_{b^*})$, while for the background processes ST, TT, DYJets and WJets are $F_{ST}(m_{b^*}), F_{TT}(m_{b^*}), F_{DYJets}(m_{b^*})$ and $F_{WJets}(m_{b^*})$ respectively. Furthermore, suppose that we are testing two hypotheses, the null hypothesis (H0) is the signal+background hypothesis ($\boldsymbol{s+b}$), i.e. we need new physics to understand the data, and the alternative hypothesis (H1) which is favored when the null hypothesis has been rejected to a sufficient degree, is the background hypothesis ($\boldsymbol{b}$), that is the data can be understood with existing physics explanations. We construct probability density functions related to the two hypotheses:

$$\begin{aligned} model0(m_{b^*};\vec{p}) = {} & p_{signal}F_{signal}(m_{b^*}) + p_{ST}F_{ST}(m_{b^*}) + p_{TT}F_{TT}(m_{b^*}) \\ & + p_{DYJets}F_{DYJets}(m_{b^*}) + p_{WJets}F_{WJets}(m_{b^*}) \end{aligned}$$

$$\begin{aligned} model1(m_{b^*};\vec{p}) = {} & p_{ST}F_{ST}(m_{b^*}) + p_{TT}F_{TT}(m_{b^*}) \\ & + p_{DYJets}F_{DYJets}(m_{b^*}) + p_{WJets}F_{WJets}(m_{b^*}) \end{aligned}$$

where $\vec{p} = \{p_{signal}, p_{ST}, p_{TT}, p_{DYJets}, p_{WJets}\}$ is a set of parameters each corresponding to the expected number of events of each process. In our analysis p_{signal} is considered as parameter of interest, while $p_{ST}, p_{TT}, p_{DYJets}, p_{WJets}$ are considered as nuisance parameters. In the figures below the probability density functions of model0 and model1 are shown together with their components and a Monte Carlo pseudo data set generated from model0 and model1 respectively.

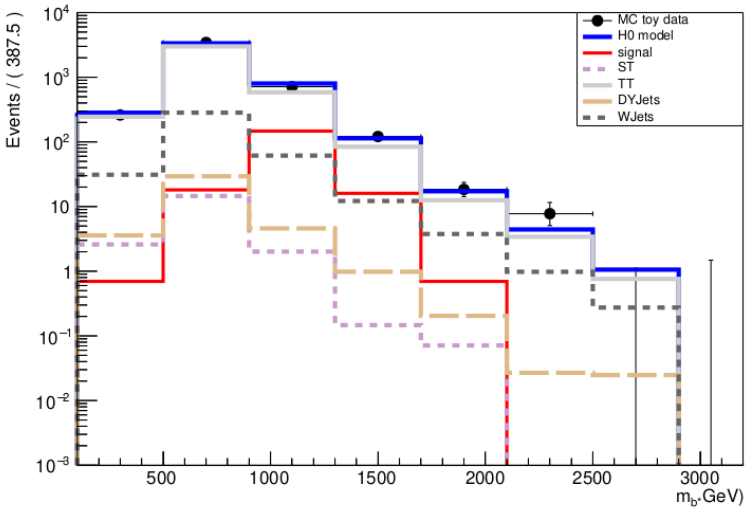

Figure 3.13: H0 hypothesis with $m_{b^*} = 1200$ GeV and its components with a MC pseudo data set generated from H0

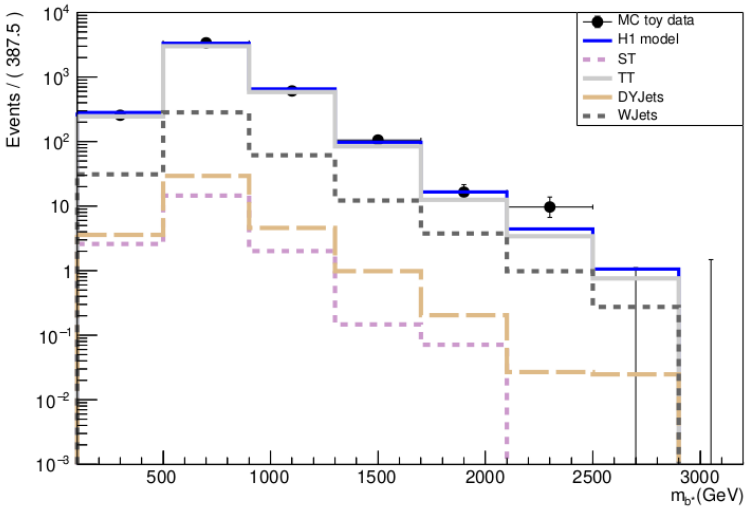

Figure 3.14: H1 hypothesis and its components with a MC pseudo data set generated from H1

The parameter of interest p_{signal} is proportional to the cross section (production rate) of the hypothesized b^* particle, since

$$p_{signal} = (\text{acceptance in MC}) \cdot \sigma \cdot L$$

The CLs method provides a means of setting upper limit on p_{signal}, and therefore on the cross section of b^* production. This is roughly done by carrying out many statistical tests for different hypothesized values of p_{signal} (different H0 models) and excluding those values (that is rejecting those H0 models) which do not fulfill the test criteria. Exclusion means that the search has given a negative result. However a negative result is not a failure of the experiment, but it gives important information that have to be expressed in a quantitative way so that theorists or other experimentalists can use them for further searches. These quantitative statements about negative results of a search for new phenomena are normally the "upper limits". By upper limit we mean a statement like the following: such a particle, if it exists, is produced with cross section below this quantity, with a certain probability.

Our goal is to set cross section upper limit for different hypothesized masses of the excited b quark. Distributions of the different hypothesized masses of b^* together with the total background distribution is shown in the figure below.

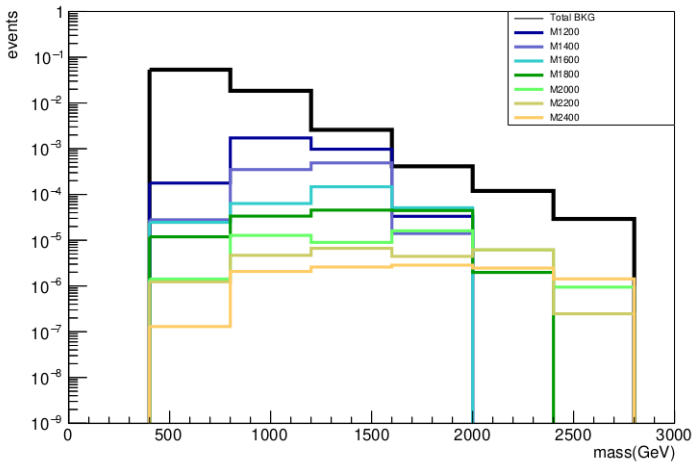

Figure 3.15: Different mass hypotheses distributions and the total background distribution

To continue, we have to choose a test-statistic, namely a quantity that distinguishes the two predictions (H0 and H1) based on their agreement with a set of data. For our analysis the likelihood ratio seems to be the best choice, constructed as follows.
The total expected number of background events is

$$N_{exp}^{bkg} = p_{ST} + p_{TT} + p_{DYJets} + p_{WJets}$$

while the total expected number of background plus signal events is

$$N_{exp}^{bkg+sig} = p_{signal} + p_{ST} + p_{TT} + p_{DYJets} + p_{WJets}$$

We generate N_{exp}^{bkg} pseudo random events from the model1, namely a pseudo data set of m_{b^*} with N_{exp}^{bkg} random values, as well as $N_{exp}^{bkg+sig}$ pseudo random events from the model0. For each data set we compute two likelihood functions, one is based on the assumption that the H0 model is true and the other is based on the assumption that the H1 model is true. Likelihood is the compatibility of the hypothesis with a given data set; but it depends on the data. Therefore we have four likelihood functions:

$$L_0(m_{b^*}|H0) = \prod_{i=1}^{N_{exp}^{bkg+sig}} model0(m_{b^*}; p_{signal}, p_{ST}, p_{TT}, p_{DYJets}, p_{WJets})$$

$$L_0(m_{b^*}|H1) = \prod_{i=1}^{N_{exp}^{bkg+sig}} model1(m_{b^*}; p_{ST}, p_{TT}, p_{DYJets}, p_{WJets})$$

$$L_1(m_{b^*}|H0) = \prod_{i=1}^{N_{exp}^{bkg}} model0(m_{b^*}; p_{signal}, p_{ST}, p_{TT}, p_{DYJets}, p_{WJets})$$

$$L_1(m_{b^*}|H1) = \prod_{i=1}^{N_{exp}^{bkg}} model1(m_{b^*}; p_{ST}, p_{TT}, p_{DYJets}, p_{WJets})$$

The test statistic we are choosing is constructed from these likelihood functions:

$$Q = -2ln\frac{L(m_{b^*}|H0)}{L(m_{b^*}|H1)}$$

For the two datasets we have two values of Q. If we repeat the process N times, that is generate the two datasets compute the four likelihood functions and then the two Q values, then we will get distributions of the test statistic, one is based on the hypothesis H0, $f(Q|H0)(= -2ln\frac{L_0(m_{b^*}|H0)}{L_0(m_{b^*}|H1)})$, and the other is based on the hypothesis H1, $f(Q|H1)(= -2ln\frac{L_1(m_{b^*}|H0)}{L_1(m_{b^*}|H1)})$. We usually call the number of repetitions N as number of toys.

Since we do not have data yet, we assume that the observed value of the test statistic is at the position where the $f(Q|H1)$ distribution gets its maximum value (we expect that the data will not be different from the background-only prediction), that is

$$f(Q_{obs}|H1) = max$$

The CLs then is computed as

$$CLs = \frac{p_{s+b}}{1 - p_b}$$

where the nominator p_{s+b} and the denominator $1-p_b$ of the CLs are shown in the figure below. (For illustrative purposes I have chosen Gaussian distributions for both $f(Q|H0)$ and $f(Q|H1)$; in our analysis the distributions of Q are not Gaussian.)

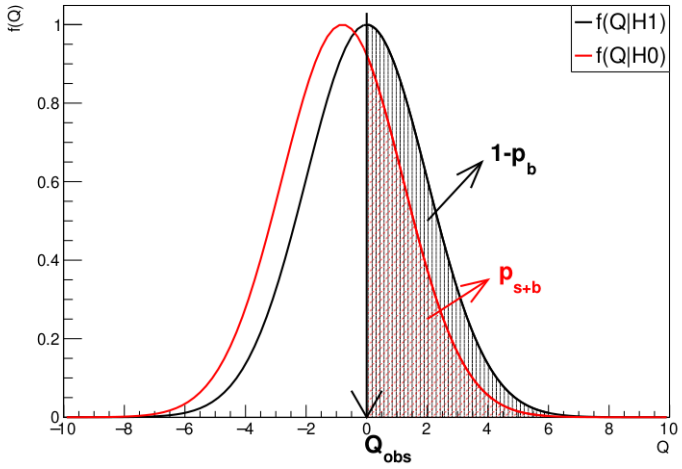

Figure 3.16: An illustrative example of the distributions of Q under H0 and H1 hypotheses showing the components for CLs computation

obviously,

$$p_{s+b} = \int_{Q_{obs}}^{\infty} f(Q|H0)$$
$$1 - p_b = \int_{Q_{obs}}^{\infty} f(Q|H1)$$

The nominator, p_{s+b}, is a measure of the compatibility of the data (here pseudo data) with the ***s+b*** hypothesis. It is the probability, under the assumption of the ***s+b*** hypothesis, of finding data equal or greater incompatibility with the predictions of the ***s+b*** hypothesis. In the denominator p_b is the probability under the assumption of ***b*** hypothesis of finding data of equal or greater incompatibility with the predictions of ***b***. $1 - p_b$ is the probability to observe a measurement that has a value larger than Q_{obs} if the background-only prediction describes the observation. This probability is a measure for the disagreement of m_{b^*} with the background only prediction.

Normally, one would carry out a standard statistical test that is based on the p-value of the s+b hypothesis, p_{s+b}. The signal model is regarded as excluded at a confidence level of $1 - \alpha = 90\%$ if one finds $p_{s+b} < \alpha$, where $\alpha = 0.1$. A confidence interval at confidence level $1 - \alpha$ for the cross section can be constructed from those values of the cross section that are not excluded, and the upper limit σ_{up} is the largest value of σ not excluded.

The problem though with the standard statistical test that is based on p_{s+b} is that one will exclude hypotheses to which one has little or no sensitivity. This corresponds to the case where the expected number of signal events is much less than that of the background; and that is the case in our analysis.

To protect against excluding models to which one has little or no sensitivity, in the CL_s procedure a signal model is regarded as excluded if one finds

$$CL_s = \frac{p_{s+b}}{1 - p_b} < \alpha$$

That is, the p-value is effectively penalized by dividing by $1 - p_b$. If one has little sensitivity to the signal model, then the two distributions are close together, the quantity $1 - p_b$ is smaller than 1, and thus the p-value of $s + b$ is penalized (increased) more. In this way one is prevented from excluding signal models in cases of low sensitivity. As previously, one takes the upper limit to be the largest value of the parameter not excluded.

From the CL_s definition one can see that CL_s is always greater than the p-value p_{s+b}. Thus the models excluded by requiring $CL_s < \alpha$ are a subset of those excluded by the usual criterion $p_{s+b} < \alpha$, and the upper limit from CL_s is therefore higher (weaker). In this sense the CL_s procedure is conservative.

Continuing our analysis, we start off with the 1200 GeV mass hypothesis and compute the CLs for different hypothesized values of the cross section. The CLs versus cross section plot is shown below:

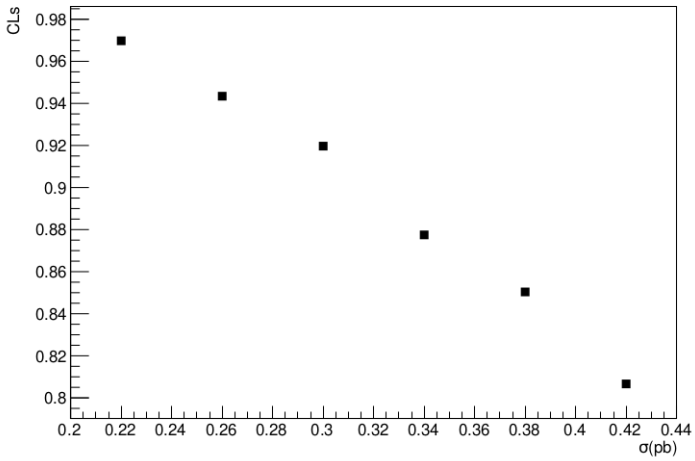

Figure 3.17: CLs versus cross section for 1200 GeV mass hypothesis

In the figures below, the corresponding distributions of the test statistics Q for the CLs computation are shown, for values of cross section 0.22 pb and 0.42 pb.

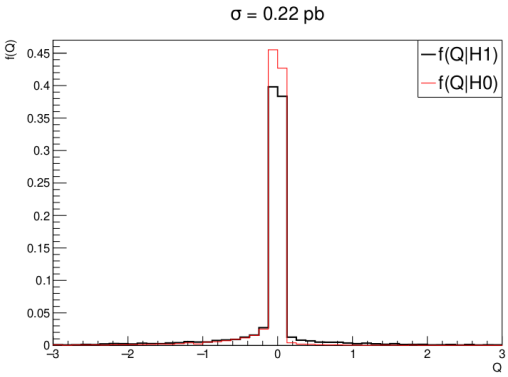

(a) Distributions of the test statistic for H0 and H1 models with an assumed cross section of the signal of 0.22 pb

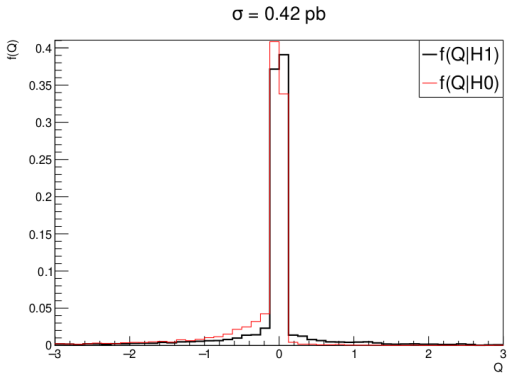

(b) Distributions of the test statistic for H0 and H1 models with an assumed cross section of the signal of 0.42 pb

Figure 3.18: An example illustrating that giving less cross section to the signal results in more overlapped distributions of the test statistic under H0 and H1 models

We notice that smaller cross section of the signal model results in more overlapped distributions of the test statistic Q, while larger cross section in more separated distributions. In our case, we regard the H0 model with its hypothesized value of σ as excluded if

$$CLs < 0.9$$

Therefore, the highest not excluded σ (cross section upper limit) is that which gives $CLs = 0.9$.

Repeating the process for different mass hypotheses, we construct the expected from Monte Carlo cross section upper limit plot for the different mass hypotheses. The plot together with the cross sections expected from theory are shown below:

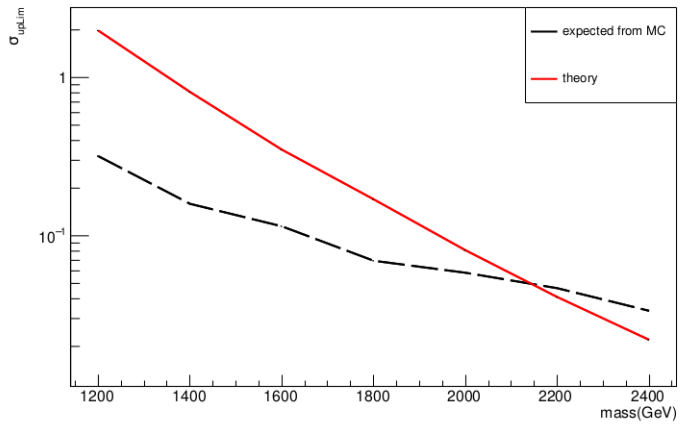

Figure 3.19: Cross section upper limit expected from Monte Carlo and cross sections predicted from theory for different mass points

From this plot we conclude that all b* mass hypotheses which have production cross section upper limit expected from Monte Carlo smaller that the cross section that the theory predicts are excluded. That is, we exclude the existence of an excited b quark with a mass below 2.2 TeV.

Our next step is to run the data though the whole analysis chain. The file containing the data is "flatTree˙SingleMuon.root". After that, we fit the

data to different H0 mass hypotheses as well as to the H1 hypothesis. The figures below show the probability density functions of model0 and model1 with their components, after fitting the data, together with the data on top.

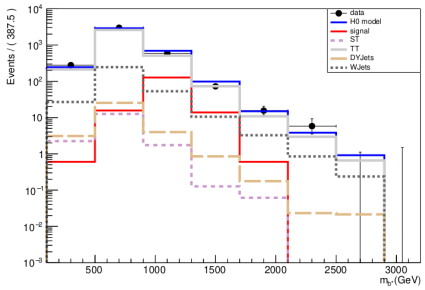

(a) Fitting data to model0 with $m_{b^*} = 1200$ GeV

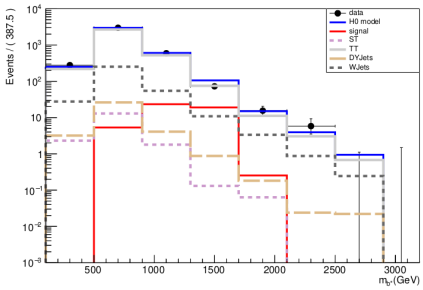

(b) Fitting data to model0 with $m_{b^*} = 1400$ GeV

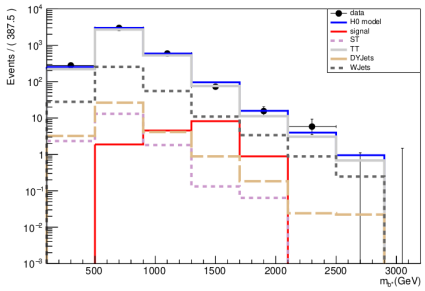

(c) Fitting data to model0 with $m_{b^*} = 1600$ GeV

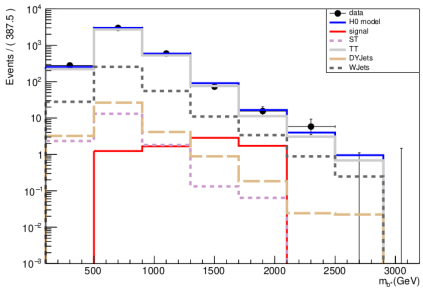

(d) Fitting data to model0 with $m_{b^*} = 1800$ GeV

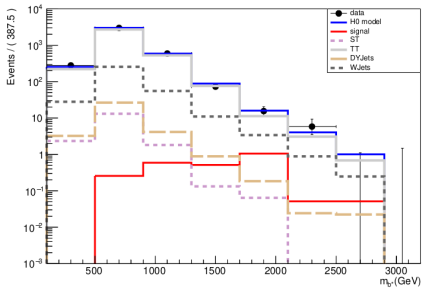

(e) Fitting data to model0 with $m_{b^*} = 2000$ GeV

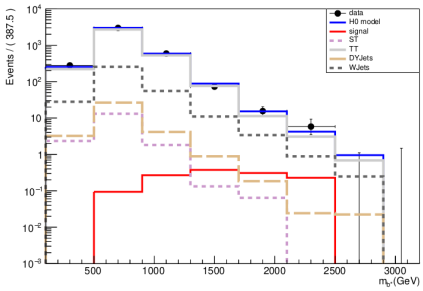

(f) Fitting data to model0 with $m_{b^*} = 2200$ GeV

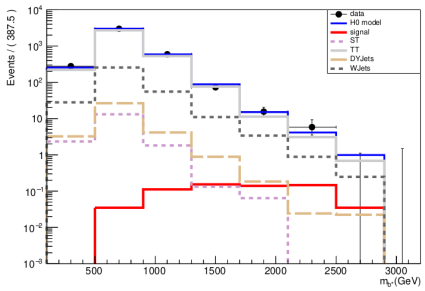

(g) Fitting data to model0 with $m_{b^*} = 2400$ GeV

Figure 3.20: Fitting data to different H0 mass hypotheses

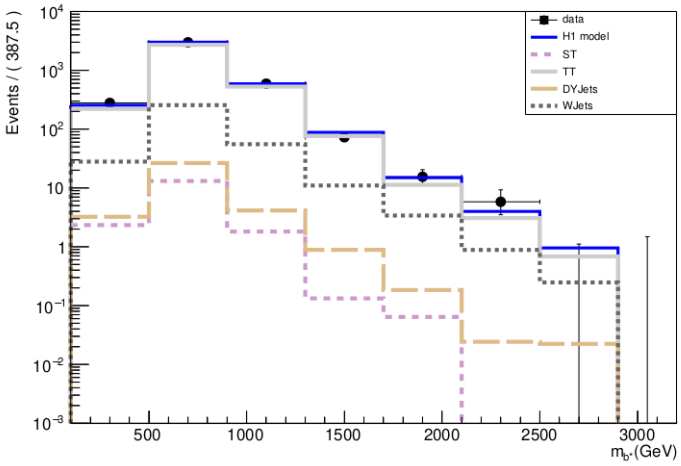

Figure 3.21: Fitting data to H1 hypothesis

We are interested to calculate what the data gives as cross section upper limit for the different H0 mass hypotheses, namely what is the observed upper limit cross section for b* production. For that, for each mass point, we fit the data to the model0 and get a minimized log-likelihood value. Similarly, we fit the data to the model1 and get another minimized log-likelihood value. Dividing these two values and multiplying with -2 we get the observed value of Q (Q_{obs}) and proceed the same way as we did with the MC toy data to compute the CLs and hence the cross section upper limit.

The yield of each process before and after fitting the data to the signal+background and fitting to the background-only model and the error of fit for different mass hypotheses are shown in the tables below:

M-1200			
process	prefit yield	postfit yield	fit error
signal	188.31	0.0378277	54.6107
ST	19.9833	200	146.426
TT	4063.53	3481.03	421.3
DYJets	40.0514	0.010292	199.201
WJets	405.828	404.355	381.033

M-1400			
process	prefit yield	postfit yield	fit error
signal	55.5717	4.65446e-05	19.45475
ST	19.9833	199.999	146.833
TT	4063.53	3484.65	421.532
DYJets	40.0514	0.0113575	199.09
WJets	405.828	400.803	363.998

M-1600			
process	prefit yield	postfit yield	fit error
signal	17.787	1.96925e-07	16.65249
ST	19.9833	199.997	146.225
TT	4063.53	3483.97	462.47
DYJets	40.0514	0.0100785	197.523
WJets	405.828	401.109	381.778

M-1800			
process	prefit yield	postfit yield	fit error
signal	8.57769	7.86749e-06	9.89723
ST	19.9833	200	146.034
TT	4063.53	3481.73	431.014
DYJets	40.0514	0.00699138	146.559
WJets	405.828	403.401	368.557

M-2000			
process	prefit yield	postfit yield	fit error
signal	2.88149	3.1931e-06	16.9899
ST	19.9833	200	145.482
TT	4063.53	3481.4	415.129
DYJets	40.0514	0.000251393	137.367
WJets	405.828	403.449	362.117

M-2200			
process	prefit yield	postfit yield	fit error
signal	1.45761	9.71185	16.7749
ST	19.9833	200	139.742
TT	4063.53	3749.92	537.862
DYJets	40.0514	125.286	136.366
WJets	405.828	0.0171102	706.688

M-2400			
process	prefit yield	postfit yield	fit error
signal	0.710754	2.43758	10.1622
ST	19.9833	199.996	142.532
TT	4063.53	3570.31	544.949
DYJets	40.0514	15.6516	177.496
WJets	405.828	296.66	639.473

If the parameter estimations with the fit method are consistent and unbiased then the pull quantity computed as

$$\text{pull} = \frac{\text{postfit value} - \text{prefit value}}{\text{fit error}}$$

must follow a Gaussian distribution with mean value 0 and standard deviation 1. A pull distribution which mean is different from zero may indicate a systematic difference between the data and the theory. If the sigma of the pull distribution is different from one then the uncertainties associated to the data could be under or over-estimated. Below the pull distribution for different mass points are shown.

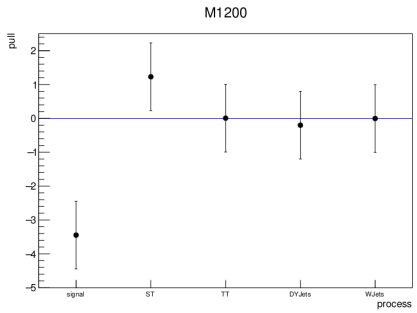

(a) $m_{b^*} = 1200$ GeV

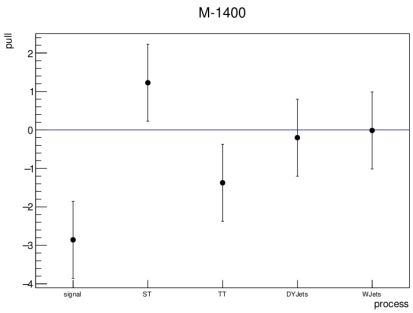

(b) $m_{b^*} = 1400$ GeV

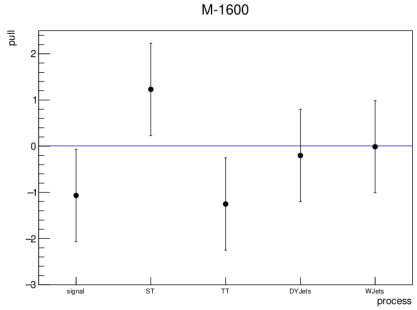

(c) $m_{b^*} = 1600$ GeV

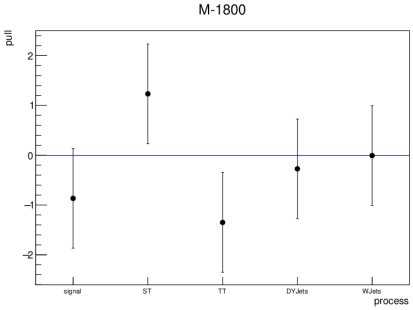

(d) $m_{b^*} = 1800$ GeV

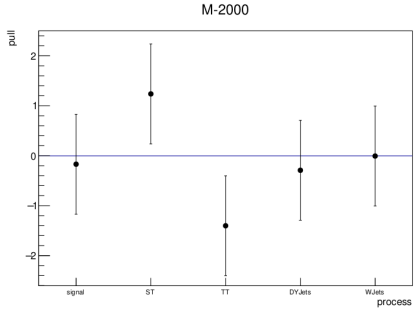

(e) $m_{b^*} = 2000$ GeV

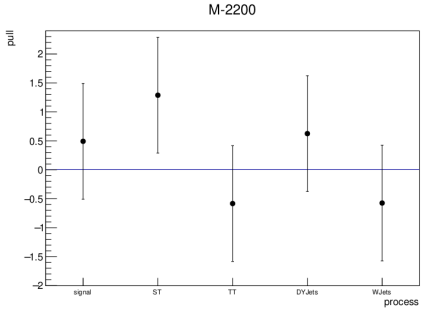

(f) $m_{b^*} = 2200$ GeV

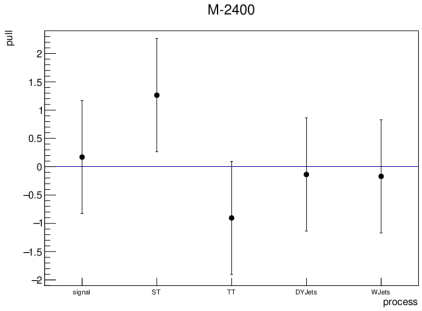

(g) $m_{b^*} = 2400$ GeV

Figure 3.22: Pull distributions for different mass points.

The observed values of the test statistic Q which the data gives for different mass points are shown in the table below.

mass (GeV)	Q_{obs}
1200	-0.000173159
1400	-0.000145615
1600	-0.000171569
1800	-0.000207935
2000	-0.000195135
2200	-0.44935
2400	-0.0676009

Finally, the observed cross section upper limit, the expected cross section upper limit and the theoretical cross section for b* production is shown in the plot below. We notice that at the 2200 GeV mass point the data gives higher upper limit than that we expect from Monte Carlo – we expect that the data will be not different from the background-only prediction. Therefore the higher observed cross section upper limit at 2200 GeV mass might be a hint that we need new physics to understand the data.

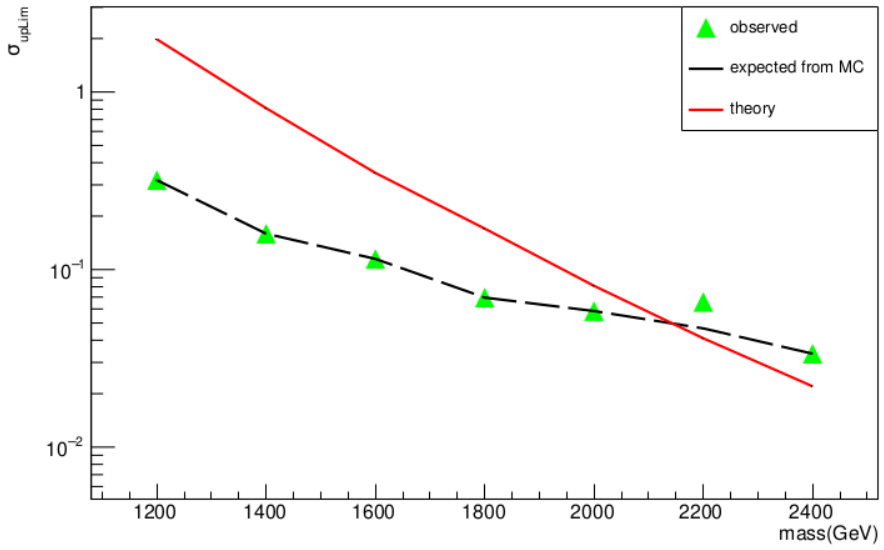

Figure 3.23: The observed cross section upper limit (green markers), the expected cross section upper limit (dashed line) and the theoretical cross sections (red line)

Conclusion

A search for an excited bottom quark that decays into a top quark and a W boson, where the top quark decays hadronically and the W boson decays leptonically, is performed using pp collisions recorded by the CMS detector at $\sqrt{s} = 13$ TeV. The dataset used corresponds to an integrated luminosity of $L = 36.3$ fb^{-1}. b^* quarks with masses below 2.2 TeV are excluded at a ?% confidence level.

Bibliography

[1] Luca Lista *Statistical Methods for Data Analysis in Particle Physics*, Second Edition

[2] Na Peng, Huaqiao Zhang, and Sarmad Masood Shaheen IHEP/UCAS *Search for singly produced b^* decaying to tW in lepton+jets(leptonic top+hadronic W) channel with CMS detector at $\sqrt{s} = 13$ GeV*

[3] Falko Dulat, Bernhard Mistlberger, Institute of Theoretical Physics, ETH Zurich, Switzerland *Limit setting procedures and theoretical uncertainties in Higgs boson searches*

[4] ATLAS Statistics Forum, 5 July, 2011 *The CLs method: information for conference speakers*

[5] Durham Ippp Workshop Paper *Presentation of search results: the CLs technique*

[6] Matthew D. Schwartz *Quantum Field Theory and the Standard Model*

[7] Stefan Schmitt, DESY *Limits in High Energy Physics*

[8] Ryan Atkin *Review of jet reconstruction algorithms*

[9] The ATLAS Collaboration *Jet reconstruction and performance using particle flow with the ATLAS detector*

[10] The CMS Collaboration *Performance of the CMS muon detector and muon reconstruction with proton-proton collisions at $\sqrt{s} = 13$ TeV*

[11] Milos Dordevic on behalf of the CMS Collaboration *The CMS Particle Flow Algorithm*

[12] The CMS Collaboration *Particle-flow reconstruction and global event description with the CMS detector*

[13] Stefan Weinzierl *Introduction to Monte Carlo methods*

[14] Torbjorn Sjostrand *Monte Carlo Generators*

[15] Tao Han *Collider Phenomenology Basic Knowledge and Techniques*

[16] Cristina Ferro *B-tagging in CMS*